

1 **Short Title:**

2 **Influence of LHCX isoforms on NPQ sites in diatoms**

3

4 **Corresponding authors:**

5 Giovanni Finazzi: giovanni.finazzi@cea.fr and Angela Falciatore: angela.falciatore@upmc.fr

6

7 **Title:**

8 **Dynamic changes between two LHCX-related energy quenching sites control diatom**
9 **photoacclimation**

10

11 Lucilla Taddei^a, Volha U. Chukhutsina^{b,c}, Bernard Lepetit^d, Giulio Rocco Stella^{a,e},

12 Roberto Bassi^e, Herbert van Amerongen^b, Jean-Pierre Bouly^a, Marianne Jaubert^a,

13 Giovanni Finazzi^f, and Angela Falciatore^a

14

15 **Affiliations:**

16 ^aSorbonne Université, CNRS, Institut de Biologie Paris-Seine, Laboratory of Computational
17 and Quantitative Biology, F-75005, Paris, France

18 ^bLaboratory of Biophysics and MicroSpectroscopy Research Facility, Wageningen University,
19 P.O. Box 8128, 6700ET Wageningen, The Netherlands

20 ^cBiophysics of Photosynthesis, Department of Physics and Astronomy, Faculty of Sciences,
21 VU University Amsterdam and LaserLaB Amsterdam, 1081 HV Amsterdam, The Netherlands

22 ^dZukunftskolleg, Department of Plant Ecophysiology, University of Konstanz, 78457
23 Konstanz, Germany

24 ^eDepartment of Biotechnology, University of Verona, 15, Strada Le Grazie, I-37134 Verona,
25 Italy

26 ^fUniversité Grenoble Alpes (UGA), Laboratoire de Physiologie Cellulaire et Végétale, UMR
27 5168, Centre National de la Recherche Scientifique (CNRS), Institut National Recherche
28 Agronomique (INRA), Commissariat à l'Énergie Atomique et aux Énergies Alternatives (CEA),
29 Institut de Biosciences et Biotechnologies de Grenoble, (BIG), CEA Grenoble, F-38054
30 Grenoble cedex 9, France

31 **One sentence summary:**

32 Multiple LHCX-related quenching sites control short- and long-term high-light acclimation
33 in the marine diatom *Phaeodactylum tricornutum*.

34 **Author contributions:**

35 A.F., G.F., H.v.A., J.P.B., M.J., B.L. and V.U.C. designed the experiments and wrote the
36 manuscript. L.T., M.J., B.L., A.F., J-P.B., and G.F., contributed to the molecular and
37 physiological analyses; G.R.S. and R.B. performed the pigment analysis; V.U.C. and H.v.A.
38 analyzed quenching features and generated decay-associated spectra. All authors discussed
39 results, revised, and approved the manuscript.

40 **Funding:**

41 This work was supported by the Marie Curie Initial Training Network Accliphot (FP7-
42 PEPOPLE-2012- ITN; 316427) to A.F., G.F., and R.B., the Agence Nationale de la Recherche
43 (ANR-12-BIME DiaDomOil) to A.F. and G.F., the Marie Curie Initial Training Network CALIPSO
44 (ITN 2013 GA 607607) to A.F., the HFSP (HFSP0052) and by the LabEx GRAL (ANR-10-LABX-
45 49-01) to G.F., and the Zukunftskolleg Konstanz and the Deutsche Forschungsgemeinschaft
46 (DFG-LE 3358/3-1) to B.L.

47

48 **Address correspondence to giovanni.finazzi@cea.fr and angela.falciatore@upmc.fr**

49

50

51

52

53

54

55 **Abstract**

56 Marine diatoms are prominent phytoplankton organisms that perform photosynthesis in
57 extremely variable environments. Diatoms possess a strong ability to dissipate excess
58 absorbed energy as heat via non-photochemical quenching (NPQ). This process relies on
59 changes in carotenoid pigment composition (xanthophyll cycle) and on specific members of
60 the light-harvesting complex (LHC) family specialized in photoprotection (LHCXs), which
61 potentially act as NPQ effectors. However, the link between light stress, NPQ, and the
62 existence of different LHCX isoforms is not understood in these organisms. Using picosecond
63 fluorescence analysis, we observed two types of NPQ in the pennate diatom *Phaeodactylum*
64 *tricornutum*, which were dependent on light conditions. Short exposure of low-light-
65 acclimated cells to high light triggers the onset of energy quenching close to the core of
66 photosystem II, while prolonged light stress activates NPQ in the antenna. Biochemical
67 analysis indicated a link between the changes in the NPQ site/mechanism and the induction
68 of different LHCX isoforms, which accumulate either in the antenna complexes or in the core
69 complex. By comparing the responses of wild-type cells and transgenic lines with a reduced
70 expression of the major LHCX isoform, LHCX1, we conclude that core-complex-associated
71 NPQ is more effective in photoprotection than is the antenna complex. Overall, our data
72 clarify the complex molecular scenario of light responses in diatoms and provide a rationale
73 for the existence of a degenerate family of LHCX proteins in these algae.

74

75

76

77 **Introduction**

78 Marine diatoms form a group of unicellular algae that dominate the phytoplankton
79 community across a wide range of ocean environments (Smetacek, 1999; de Vargas et al.,
80 2015; Malviya et al., 2016). Their environmental success likely reflects their capacity to
81 respond to numerous environmental challenges, including changes in nutrient levels and
82 light. While the mechanisms of the responses of diatoms to nutrients have been studied in
83 detail (Allen et al., 2008; Allen et al., 2011; Marchetti et al., 2012; Alipanah et al., 2015;
84 Morrissey et al., 2015; Matthijs et al., 2016; McQuaid et al., 2018), little is known about light
85 acclimation responses. Like most photosynthetic organisms, diatoms optimize light capture
86 by enhancing their absorption capacity at low intensities, and by down-regulating the
87 utilization of absorbed light at oversaturating energy fluxes (Müller et al., 2001; Eberhard et
88 al., 2008). The latter process is triggered by the induction of the high-energy quenching (qE)
89 component of non-photochemical quenching (NPQ) (Horton et al., 1996). qE reflects the
90 increased thermal dissipation of excess light following the activation of qE effector proteins
91 in photosystem II (PSII) and changes in the pigment composition (via carotenoid de-
92 epoxidation through the xanthophyll cycle, XC). qE effectors include the small PSII subunit
93 (PsbS) in plants and members of the light-harvesting complex stress-related (LHCSR) family
94 in microalgae and mosses (Peers et al., 2009; Alboresi et al., 2010; Ballottari et al., 2016).
95 The qE machinery of diatoms differs from that of plants and green algae in two main aspects.
96 Diatoms possess two xanthophyll cycles catalyzing the de-epoxidation of diadinoxanthin
97 (DD) to diatoxanthin (DT) and of violaxanthin (V) to zeaxanthin (Z) (Lohr and Wilhelm, 1999).
98 Moreover, their qE effectors belong to the light-harvesting complex (LHC) family specialized
99 in photoprotection, the LHCX, (Bailleul et al., 2010; Zhu and Green, 2010; Ghazaryan et al.,
100 2016), which is related, but not identical, to the LHCSR family. Multiple LHCX genes exist in

101 diatoms and gene expression studies indicate that the four *Phaeodactylum tricornutum* LHCX
102 isoforms differentially accumulate in the thylakoids upon exposure to different
103 environmental stresses due to the existence of multiple regulatory control pathways (Allen
104 et al., 2008; Nymark et al., 2009; Bailleul et al., 2010; Lepetit et al., 2013; Lepetit et al.,
105 2017). These findings suggest that the functional diversity of the LHCX proteins may expand
106 the diatom's capacity to respond to the highly variable ocean environments (Zhu and Green,
107 2010; Taddei et al., 2016; Lepetit et al., 2017).

108 In this work, we combined biochemical and spectroscopic approaches to address the role
109 of the different LHCXs in photoprotection. We found that low-light (LL) -acclimated cells
110 display a qE mainly driven by energy quenching in close proximity to the reaction center of
111 PSII (the PSII core) and, to some extent, in the antennas (also called Fucoxanthin Complex
112 Binding Proteins, FCPs). This qE is largely controlled by LHCX1, which is present in both the
113 PSII core and the FCP complexes. On the other hand, prolonged exposure to high light (HL)
114 enhances FCP localized quenching. Biochemical analysis suggests that this shift is related to
115 the induction of other LHCX isoforms, which accumulate in the antenna but not in the PSII
116 core. By comparing the physiological responses of wild-type (hereafter called WT) and
117 knock-down lines with reduced content of the LHCX1 isoform, we conclude that qE antenna
118 quenching is less effective than core qE in protecting cells from light damage. Overall, by
119 relating different qE mechanisms to different molecular actors, we propose a detailed model
120 for diatom NPQ, which is one of the key elements of the environmental flexibility of these
121 algae in modern oceans.

122

123

124

125 **Results**

126 ***The LHCX1 knock-down line recovers WT-NPQ levels upon prolonged high-light exposure.***

127 In *P. tricornutum*, LHCX1 is the only member of the *LHCX* gene family that is substantially
128 expressed in cells grown in LL (30 $\mu\text{mol photons m}^{-2}\cdot\text{s}^{-1}$, 12:12 h light:dark cycle) (Bailleul et
129 al., 2010; Taddei et al., 2016; Lepetit et al., 2017). In these conditions, LHCX1 is the main
130 NPQ effector. This role is evidenced by the phenotype of a transgenic line with down-
131 regulated expression of *LHCX1* (hereafter named *lhcx1*), which contained less LHCX1 and
132 showed a lower qE capacity than the WT when grown in LL (Bailleul et al., 2010) (Fig. 1A and
133 Supplemental Fig. S1). Exposure to HL (500 $\mu\text{mol photons m}^{-2}\cdot\text{s}^{-1}$, 12:12 h light:dark cycle,
134 Fig. 1B) for two days enhanced NPQ in both WT and transgenic cells. However, the NPQ
135 increase was larger in the mutant, and therefore, the quenching capacity of the two strains
136 became indistinguishable in HL. Immunoblot analysis of HL-treated cells showed that LHCX1
137 levels were increased in both strains, even if the *lhcx1* knock-down cells maintained a lower
138 LHCX1 content than the WT cells (Fig. 1C). This observation suggests that the increase in
139 LHCX1 alone cannot account for the observed difference in NPQ amplitude in LL- and HL-
140 treated cells. To further elucidate the effect of quenching on antenna protein domains, we
141 compared the XC pigments in WT and *lhcx1* cells in LL and HL and found a similar DD/DT
142 content in LL-treated cells (Supplemental Table S1), which was in agreement with previous
143 results (Bailleul et al., 2010). HL triggered a significant increase of DD+DT but also led to the
144 appearance of violaxanthin (V), antheraxanthin (A) and zeaxanthin (Z), i.e. xanthophyll
145 precursors of DD+DT synthesis under HL stress (Lohr and Wilhelm, 1999). The *lhcx1* knock-
146 down line displayed a slightly increased amount of total DD+DT compared to the WT, while

147 its de-epoxidation state was the same as of the WT. This increase of DT could, in principle,
148 account for the recovery of WT-like NPQ levels in the *lhcx1* cells. Nevertheless, previous
149 work has shown that induction of DT by prolonged light stress cannot enhance NPQ without
150 a concomitant increase of LHCX proteins (Bailleul et al., 2010; Lepetit et al., 2013; Lepetit et
151 al., 2017). On the other hand, we detected a substantial accumulation of LHCX3 in both
152 strains in HL (Fig. 1C). Induction of the LHCX2 isoform was also visible at the mRNA level (Fig.
153 1E), and at the protein level after over-exposure of the western blot membrane (Fig. 1D).
154 Because of their possible role in NPQ, this finding prompted us to further investigate the link
155 between the induction of these proteins and the acquirement of WT levels of NPQ in HL-
156 grown *lhcx1* cells.

157

158 **Different quenching capacities in LL- and HL-treated cells reflect a heterogeneous**
159 **distribution of the LHCX isoforms in different chloroplast fractions.** Previous studies have
160 localized LHCX1 either in the FCP complexes (Lepetit et al., 2010; Schaller-Laudel et al., 2015)
161 or in photosystem I (PSI) (Grouneva et al., 2011). However, no information is available for
162 the other LHCX isoforms. Therefore, we reinvestigated the localization of the various LHCX
163 proteins in the different photosynthetic complexes isolated by sucrose density gradient
164 centrifugation (Fig. 2A) from detergent-treated thylakoid membranes of *P. tricornutum*. Five
165 distinct fractions were recovered from LL- and HL-treated WT and *lhcx1* strains (Fig. 2A).
166 Using western blot analysis, we identified them as free pigments, trimeric FCPs (i.e. the
167 physiological antenna form in *P. tricornutum* (Lepetit et al., 2007; Joshi-Deo et al., 2010;
168 Gardian et al., 2014), PSII monomers (PSII m), PSI, and PSII dimers (PSII d) in accordance with
169 earlier results obtained with clear native polyacrylamide gel electrophoresis (PAGE) (Nagao

170 et al., 2013). LHCX1, the only isoform strongly expressed in LL-treated cells, is ubiquitous as
171 it co-localizes with the FCP and PSI as well as with the PSII dimer fractions (Fig. 2B). As
172 expected, samples isolated from *lhcx1* cells had a lower content of this protein. On the other
173 hand, LHCX3, which is induced in HL-treated cells (Nymark et al., 2009; Bailleul et al., 2010;
174 Lepetit et al., 2013; Taddei et al., 2016; Lepetit et al., 2017), seems to have a more specific
175 localization, being found only in the FCP and PSI fractions (Fig. 2B). The LHCX2 isoform could
176 not be detected by western blot analysis, likely because of a lower level of accumulation as
177 compared to LHCX3 in prolonged HL stress and a lower affinity of the antibody generated
178 against the Chlamydomonas LHCSR3 for this isoform.

179

180 **Prolonged exposure to HL induces a change in the NPQ quenching site in *P. tricornutum***
181 **cells.**

182 We employed picosecond spectrally-resolved fluorescence measurements to analyze the
183 quenching features in LL- and HL-treated WT and *lhcx1* cells. To discriminate between
184 quenching in the antennas and PSII cores, we selectively excited different pigment
185 populations. We excited fucoxanthin (FX), which is only found in the FCP antenna complexes
186 (Lepetit et al., 2010), with 540-nm light. Conversely, we used 400-nm light to excite
187 chlorophyll *a* (Chl *a*) (Szabó et al., 2008; Chukhutsina et al., 2013), which is present in PSI and
188 PSII cores and in the FCPs. Time-resolved fluorescence emission data were globally fitted to
189 obtain the fluorescence lifetimes and the corresponding decay-associated spectra (DAS).

190 Global analysis of time-resolved fluorescence data was performed in WT and *lhcx1*
191 lines in LL (Fig. 3) and HL (Fig. 4) excited at 400 and 540 nm, both in the quenched and
192 unquenched states. We found that five components are required for accurately describing

193 the fluorescence kinetics in LL (Fig. 3) and the results on WT cells upon excitation with 400
194 nm light are described in more detail below. The three components with the shortest
195 lifetimes (14 ps, 64 ps, and 242 ps) mainly reflected excitation energy transfer from short-
196 wavelength (high-energy) pigments to long-wavelength (low-energy) pigments. This downhill
197 energy transfer could easily be recognized because the corresponding DAS were positive on
198 the short-wavelength side and negative on the long-wavelength side (Van Stokkum et al.,
199 2008). For example, the 14-ps DAS displayed a positive band at 675 nm and two negative
200 bands at 690 nm and 717 nm. This reflected excitation energy transfer (EET) from
201 chlorophyll (Chla) with fluorescence peaking around 675 nm (Chl₆₇₅) to Chl₆₉₀ and Chl₇₁₇, and
202 mainly represented EET from FCPs to both photosystems, and possibly Lhcf15, a member of
203 the Fucoxanthin Chlorophyll a/c binding Protein family (Chukhutsina et al., 2014). Indeed,
204 the peak position of Chl₇₁₇ strongly resembled that of the red (long-wavelength) antennas
205 composed of Lhcf15, which emit at 716 nm at 77 K (Herbstová et al., 2015; Herbstová et al.,
206 2017). The assignment of this long-wavelength emission (to PSI or Lhcf15, or both) is further
207 discussed in the next section. The second DAS represented a similar process occurring on a
208 slower timescale (64 ps). The 242-ps (3rd) DAS reflected energy equilibration between Chl₆₈₇
209 and Chl₇₁₇, and surprisingly, was an order of magnitude slower than observed previously for
210 FCPs of *Cyclotella meneghiniana* (Chukhutsina et al., 2014). This suggested that the red
211 antennas are part of a large antenna system, in which it takes a relatively long time to reach
212 some of the red-emitting species. The 894-ps DAS represented fluorescence decay processes
213 in PSII and PSI emitting at 690 nm and 712 nm, respectively. The 4-ns DAS, emitting at 717
214 nm, again reflected relaxation of the “red-most” emitters of *P. tricornutum*. Fig. 3 also shows
215 the results for LL-treated WT cells in which NPQ has been induced. In this case, we found
216 similar lifetimes (14 ps, 61 ps, 219 ps, 816 ps, and 4 ns) as for unquenched cells (Fig. 3,

217 Supplemental Table S2) but the DAS are different. The 14-ps spectrum was virtually identical
218 for the quenched and unquenched sample, including the EET part to the long-wavelength
219 pigments (Fig. 3). On the other hand, the 61-ps and 219-ps components showed strongly
220 reduced EET to the long-wavelength band. As a result, the amplitude of the 4-ns DAS
221 decreased substantially, corresponding to a decrease of the average fluorescence lifetime
222 (Supplemental Table S3) and quenching of the fluorescence. We directly compared the
223 “steady-state” fluorescence spectra, which have been reconstructed from the DAS as
224 explained in Materials and Methods. The resulting quenched and unquenched spectra for LL-
225 treated WT cells are presented in Fig. 5A. Both spectra were dominated by the red-shifted
226 fluorescence band around 717 nm, but the spectrum corresponding to the NPQ state was
227 substantially smaller. We also observed quenching of the 687-nm emission (Fig. 5 insert).

228 The same measurements were performed with a 540-nm excitation to preferentially
229 excite the antenna (Fig. 3B), and the obtained DAS were very similar to those obtained upon
230 the 400-nm excitation (see Fig. 3A). Also, the reconstructed steady-state spectra for
231 quenched and unquenched cells (Fig. 5B) were very similar to those obtained with 400-nm
232 excitation.

233 Time-resolved fluorescence measurements were also performed on LL-treated *lhcx1* cells
234 and the results for unquenched cells were very similar to those of WT cells (Fig. 3, C and D).
235 The spectra for the quenched cells were also reminiscent of those of the WT cells. However,
236 the amount of quenching was smaller as can be seen for the reconstructed steady-state
237 spectra in Fig. 5 (C and D). Moreover, quenching of the 687-nm emission was not present in
238 the transgenic cells (Fig. 5 inserts). It is important to note that the differences induced by
239 NPQ cannot be directly compared to those obtained during fluorescence induction

240 measurements, which were performed at room temperature (RT) (Fig. 1). Indeed, the
241 fluorescence steady state emission (Fig. 5) calculated at 77K was dominated by the long-
242 lived PSI fluorescence or other red-most emitting species, at variance with fluorescence
243 measured at room temperature.

244 Similar measurements were then performed on HL-treated cells (Fig. 4). Four decay
245 components were sufficient to fit the data for both types of cells upon excitation with either
246 400 nm or 540 nm. In contrast to the results on LL-treated cells, there were substantial
247 differences between the two excitation wavelengths, which were clearly visible when
248 comparing the reconstructed steady-state spectra (Fig. 5 E to H). Excitation of the antenna at
249 540 nm led to enhanced fluorescence quenching (Fig. 5F) as compared to the 400-nm
250 excitation (Fig. 5E), and this was also observed for the *lhcx1* cells (Fig. 5 G and H). Therefore,
251 it can be concluded that in HL-treated cells, a substantial portion of the quenching is
252 localized in the FCPs. Earlier studies using time-resolved fluorescence (Miloslavina et al.,
253 2009; Chukhutsina et al., 2014) identified two quenching sites in diatoms. The first one (Q1)
254 was mainly localized in the antenna complexes that detach from the photosystems during
255 quenching. The second one (Q2) was found in close proximity to the PSII core (Chukhutsina
256 et al., 2014). In the frame of this model, our data suggest that Q1 quenching becomes more
257 prominent in *P. tricornutum* cells under HL conditions. Under LL conditions, this antenna-
258 related quenching is not observed and we conclude that the WT cells (and to a far lesser
259 extent, the *lhcx1* cells) develop NPQ mainly based on Q2 localized quenching.

260 Overall, the results of picosecond fluorescence decay spectroscopy and biochemistry
261 suggest that LHCX1 is responsible for the large NPQ associated to the PSII core that is
262 observed in LL. Hence, LHCX1 is mandatory for Q2. Conversely, the onset of the “extra”

263 antenna-related NPQ observed in HL-exposed cells (Q1) should be due to the specific
264 induction of other LHCX isoforms, such as LHCX3, predominantly detected in the antenna
265 fraction.

266

267 **Consequences of “antenna-” and “PSII core-” localized quenching on light acclimation of *P.***
268 ***tricornutum* cells.** Based on the conclusions from the picosecond fluorescence
269 measurements (i.e. the preferential detection of “antenna” (Q1) and “PSII core” (Q2)
270 quenching in diatoms in HL and LL conditions, respectively), we tried to evaluate the relative
271 efficiency of the two quenching mechanisms in protecting the photosynthetic apparatus
272 from photodamage. To this aim, we compared the photosynthetic performances of WT and
273 *lhcx1* cells grown either in LL, where the “PSII core” quenching is mostly active, or in HL,
274 where antenna quenching becomes the prominent component of NPQ.

275 A shift from LL to HL for two days largely increased the photosynthetic activity of WT
276 cells, indicating that the cells properly acclimate to the higher photon flux (Fig. 6 A) and
277 therefore sustain growth (Supplemental Fig. S2). In parallel to the increased photosynthesis,
278 respiration was also enhanced (Supplemental Table S4) as expected because of the tight link
279 between the two processes in diatoms (Bailleul et al., 2015). On the contrary, *lhcx1* cells
280 were unable to increase their photosynthetic and respiratory capacities upon HL exposure
281 for two days (Fig. 6B and Supplemental Table S4). By calculating PSII inactivation (either from
282 changes in the Fv/Fm ratio or using the $1/F_o - 1/F_m$ parameter (Campbell and Tyystjärvi,
283 2012), we observed a stronger photoinactivation in *lhcx1* knock-down cells compared to the
284 WT (Supplemental Table S4) when exposed to HL. This also suggested that despite the
285 similar NPQ capacity of both cell lines in HL, *lhcx1* cells were more prone to photoinhibition

286 than the WT. This conclusion was supported by a biochemical analysis of the thylakoid main
287 complexes using antibodies for the LHCX proteins, the PSII (D2) and PSI (PsaF)
288 photosynthetic subunits (Fig. 6, C and D), and the ATPase complex subunit (β CF1). We found
289 that both genotypes displayed reduced levels of PSII and PSI proteins upon exposure to HL
290 for 2 days. Overall, these data confirm that *P. tricornutum* responds to increasing light
291 intensities by reducing the number of reaction centers, a strategy known in diatoms and
292 other microalgae as the n-type photoacclimation (Falkowski and Owens, 1980). However,
293 the effect on PSII was exacerbated in the *lhcx1* cells, suggesting that PSII was specifically
294 degraded upon the high light shift in *lhcx1* as a consequence of photoinhibition.

295

296 **Discussion**

297 Our biochemical, spectroscopic, and physiological investigation suggests a model for
298 photoprotection in *P. tricornutum* (Fig. 7), in which the differential accumulation of LHCX
299 isoforms in different photosynthetic complexes modulates the efficiency of NPQ via different
300 quenching mechanisms. We show that two main LHCX isoforms present in the light (LHCX1
301 and LHCX3 (Taddei et al., 2016)) are located in different regions in the photosynthetic
302 complexes of this alga. While LHCX1 is ubiquitously distributed in PSI, PSII, and the FCPs,
303 LHCX3 is only associated with the PSI and FCP complexes. Moreover, LHCX1 and LHCX3 are
304 differentially expressed depending on the light regime. LHCX1 is the predominant isoform in
305 LL, while LHCX1 and LHCX3 accumulate in HL-exposed cells. We suggest that in LL-acclimated
306 cells, LHCX1 would provide a constitutive NPQ capacity mainly localized near the PSII core
307 (Q2 (Miloslavina et al., 2009; Chukhutsina et al., 2014)) where LHCX1 is found (Fig. 7). The
308 existence of a link between this quenching and LHCX1 is supported by the finding that the
309 NPQ amplitude is reduced when the content of LHCX1 is diminished, e.g. in the *lhcx1* knock-

310 down line, in the Pt4 ecotype, and also in WT cells at the end of the day (Bailleul et al.,
311 2010). In addition to this “basal” quenching process, an additional quenching is observed
312 upon HL exposure for a few days (Lepetit et al., 2013; Lepetit et al., 2017). This quenching is
313 mostly localized in the FCPs, and therefore corresponds to the previously identified Q1 type
314 of quenching (Miloslavina et al., 2009; Chukhutsina et al., 2014). In the antenna, Q1 would
315 benefit from the additional presence of the HL-inducible LHCX3 isoform (Fig. 7), and possibly
316 the LHCX2 isoform in this process, which also accumulates to some extent under HL stress
317 (Taddei et al., 2016; Lepetit et al., 2017).

318 Our physiological data also allowed us to assess the relative efficiency of the two LHCX-
319 related NPQ mechanisms. While both the WT and *lhcx1* lines have a comparable NPQ
320 capacity in HL, *lhcx1* cells are more prone to photoinhibition. However, antenna quenching,
321 Q1, is prominent in cells with a deregulated LHCX1 expression, while Q2 quenching (“PSII
322 core” quenching) dominates in the WT. Overall, this observation suggests that “PSII core”
323 quenching is more efficient in protecting diatoms against photoinhibition of PSII, as recently
324 hypothesized (Kuzminov and Gorbunov, 2016; Giovagnetti and Ruban, 2017). In the frame of
325 this model, the differences in NPQ (Fig. 1) and photosynthesis (Fig. 6) between WT and *lhcx1*
326 cells in LL vs. HL conditions can be explained based on the presence of distinct complexes
327 that are differentially quenched by members of the LHCX family.

328 Consistent with the above scenario, previous studies have revealed a fine-tuning of
329 qE based on changes in the amount/localization of the qE protein effectors in other
330 photosynthetic organisms. In plants, Bergantino and colleagues have proposed that PsbS
331 could trigger different types of NPQ via its association with either the PSII core or the LHCII
332 (light harvesting complex II) antenna complexes (Bergantino et al., 2003). This would occur

333 via a hypothesized protein monomerization, which has recently been experimentally
334 observed *in vitro* (Fan et al., 2015). Consistent with this idea, a fast-developing NPQ is lost in
335 the NoM mutant lacking PSII core-bound monomeric LHCs, while the slow-developing
336 quenching was unaffected (Dall'Osto et al., 2017). In green algae, differential binding of
337 LHCSR3 to PSI and PSII has been reported and related to changes in NPQ (Allorent et al.,
338 2013). Recently, Pinnola and colleagues have also shown that PSI-bound LHCSR1 induces
339 NPQ in this complex (Pinnola et al., 2015) in the moss *Physcomitrella patens*. Our findings
340 that LHCX3 is bound to PSI are consistent with the occurrence of a similar quenching process
341 in diatoms as well. However, testing this possibility is difficult in diatoms due to the peculiar
342 nature of the long-wavelength fluorescence band around 717-720 nm, which is seen in *P.*
343 *tricornutum* cells, especially in LL-treated cells. In plants and green algae, PSII and PSI
344 fluorescence emission can be easily distinguished by their spectral features and lifetimes,
345 with PSI emitting at longer wavelengths with a shorter lifetime. In diatoms, the 717-720 nm
346 band has been attributed to emission by a PSII-associated red-shifted antenna (Herbstová et
347 al., 2015; Herbstová et al., 2017). In our global analysis of WT cells excited at 400 nm, we
348 observed 3 DASs that show EET towards the long-wavelength pigments. The fastest
349 component of 14 ps is characteristic for EET in PSI and is observed for PSI from the plant
350 *Arabidopsis thaliana* (Wientjes et al., 2011; Tian et al., 2017) and the green alga
351 *Chlamydomonas reinhardtii* (Ünlü et al., 2016; Włodarczyk et al., 2016). The observed time
352 constants for the major part of the transfer range from 5-11 ps in *A. thaliana* to 7-29 ps in *C.*
353 *reinhardtii*, which is similar to the 14 ps observed for LL-treated WT unquenched cells. The
354 other components reflecting EET to the long-wavelength pigments are far slower (64 and
355 242 ps) than usually observed for PSI and we ascribe them to transfer to Lhcf15 proteins,
356 which are known to emit at 716 nm at 77K (Herbstová et al., 2015; Herbstová et al., 2017). It

357 is also worthwhile to mention that no nanosecond component with PSI characteristics has
358 been observed for diatoms (Chukhutsina et al., 2014), in contrast to what has been reported
359 for native membranes of higher plants or cyanobacteria, where DAS with 2-ns and 7.4-ns
360 lifetimes represent slow PSI trapping from red pigments (van der Weij-de Wit et al., 2011;
361 Chukhutsina et al., 2015). Interestingly, when NPQ is induced in the LL-treated WT cells, the
362 fastest DAS remains entirely unchanged as well as the 14-ps lifetime. This finding suggests
363 that LHCX1 does not induce quenching of PSI but rather induces quenching on the red-
364 shifted antennas of PSII. Consistent with this, transfer to the long-wavelength pigments of
365 Lhcf15 is reduced considerably, leading to substantial quenching of their fluorescence. The
366 results obtained for the 540-nm excitation are also consistent with this picture and the same
367 is true for the results on LL-treated *lhcx1* cells. When the cells are grown in HL, the long-
368 wavelength fluorescence is strongly reduced. However, upon induction of NPQ, the long-
369 wavelength band is also quenched. Again, no clear difference is observed in the fastest DAS,
370 which corresponds to EET to the long-wavelength band, while quenching is mainly due to the
371 reduction of the 4-ns component. These findings might suggest that like LHCX1, LHCX3 does
372 not induce NPQ in PSI but rather in the red-shifted antennas of PSII, although the possibility
373 of quenching in PSI cannot be unambiguously ruled out.

374 Overall, we propose that active regulation of the two forms of quenching by different
375 LHCX isoforms provides a rationale for the existence of several isoforms of these qE
376 effectors, their number being, on average, larger than that found in all the other algal
377 species studied thus far (see (Taddei et al., 2016; Mock et al., 2017)). Multiple regulation of
378 the LHCX family members by nutrient starvation (Taddei et al., 2016) and other stresses
379 (e.g., light fluctuation (Lepetit et al., 2017) and prolonged darkness (Taddei et al., 2016))
380 would provide additional degrees of flexibility in controlling responses to environmental

381 changes, as required for efficient acclimation to the continuous changes of the ocean
382 environment.

383

384 **Materials and Methods**

385 **Strains and culture conditions:** Axenic *P. tricornutum* (Pt1 8.6, CCMP2561) wild type and
386 the *lhcx1* knock-down (Bailleul et al., 2010) strains were grown in f/2 medium at 19°C in a
387 12-h-light:12-h-dark photoperiod. Cells were first acclimated to 30 $\mu\text{mol photons m}^{-2}\cdot\text{s}^{-1}$ (LL)
388 and then shifted to 500 $\mu\text{mol photons m}^{-2}\cdot\text{s}^{-1}$ (HL) white light for two days. Cells were
389 collected during the exponential phase of growth.

390 **Oxygen evolution and consumption:** Rates of oxygen evolution and consumption were
391 measured with a Clark electrode (Hansatech, UK) at different light intensities (0, 90, 200,
392 450, 750, and 2300 $\mu\text{mol photons m}^{-2}\cdot\text{s}^{-1}$) and the measurement was performed when the
393 signal was stable. Illumination was maintained for 2 minutes at every intensity to attain
394 steady-state oxygen evolution while avoiding an excessive illumination that could lead to
395 photoinhibition. Net photosynthesis was calculated as light-driven oxygen evolution minus
396 dark respiration.

397 **Pigment analysis:** Pigment extraction was performed on cells grown either in LL or HL for
398 two days. Cells were irradiated for 10 min with strong HL before being collected by quick
399 filtration. Pigments were extracted on ice using 96% ethanol, buffered with Na_2CO_3 , in the
400 dark for 30 minutes and centrifuged. The supernatant was loaded in a high-performance
401 liquid chromatograph (Thermo-Fisher) with a detector diode array to analyze the visible
402 region with a C18 spherisorb column (7.3 x 30mm) using an aqueous mixture of
403 acetonitrile/methanol/0.1 M Tris-HCl buffer (pH 8.0) (72:8:3, v:v:v, buffer A) and a

404 methanol/hexane mixture (4:1, v:v, buffer B). The runs were done at a flux of 1.5 mL,
405 starting with 100% buffer A: 0-5 min 97% A, 5-17 min a gradient to 80% A, 17-18 min to
406 100% of buffer B, 18-23 min 100% B. Pigments are distinguishable by the retention time and
407 by the absorption spectrum. The de-epoxidation state was calculated as $(Z+1/2 A)/(Z+A+V)$
408 or as $(DT)/(DT+DD)$ (Ruban et al., 2004; Bonente et al., 2011).

409 **Isolation of pigment-protein complexes:** Thylakoid membrane isolation and solubilization
410 was conducted following the protocol by Lepetit et al., 2007. Equal amounts of isolated
411 thylakoids, corresponding to 0.5-1 mg of total chlorophyll, were solubilized with n-dodecyl β -
412 D-maltoside (DM, Carl Roth, Germany) at detergent/chlorophyll ratios of 30 corresponding
413 to 3% DM (w/v). The solubilized thylakoids were immediately applied to linear sucrose
414 gradients (from 0 to 0.6 M sucrose (w/v) in isolation medium B complemented with 0.03%
415 DM. Samples were centrifuged for 17 h at 110,000 g using a swing-out rotor. After the
416 separation, sucrose gradient bands were harvested with a syringe and stored for further
417 characterization at -20°C.

418 **Expression analyses:** Total RNA were extracted and analyzed by RT-qPCR as described
419 (Taddei et al., 2016). Total proteins were extracted and analyzed by western blot as
420 previously described (Bailleul et al., 2010). Proteins from photosynthetic complexes were
421 analyzed by charging equal amounts of chlorophyll (1 μ g), quantified according to Lohr and
422 Wilhelm (Lohr and Wilhelm, 2001). Proteins were detected by specific antibodies: anti-
423 LHCSR (dilution 1: 5000, gift of Prof. G. Peers, University of California, Berkeley, CA, USA),
424 anti-D2 (dilution 1:10,000; gift of Prof. J.-D. Rochaix, University of Geneva, Switzerland), anti-
425 PsaF and anti- β CF1 for the chloroplastic ATPase (dilution 1:1000 and 1:10,000, respectively,
426 gifts of F.-A. Wollman, Institut de Biologie Physico-Chimique, Paris, France), and anti-LHCF1-
427 11 (dilution 1:2000, gift of Prof. C. Büchel, Institut für Molekulare Biowissenschaften

428 Universität Frankfurt, Frankfurt, Germany). Densitometry measurements of each protein
429 signal were performed using ImageJ (Schneider et al., 2012). Protein signals in the linear
430 range of detection were adjusted for loading according to the corresponding β CF1 signal,
431 and values were normalized to the value of the WT in the LL condition.

432 **Room-temperature chlorophyll fluorescence measurements:** The kinetics of chlorophyll
433 fluorescence yields at room temperature were measured using a fluorescence CCD camera
434 recorder (Speezen1, JBeamBio, France (Johnson et al., 2009)) on cells at 1×10^6 to 2×10^6
435 cells/ml. Before the measurements, all samples were adapted to ambient, dim light for 15
436 min at 18°C to relax the reaction centers. The F_v/F_m ratio was calculated as $(F_m - F_o)/F_m$,
437 where F_m and F_o are the maximum and the minimum fluorescence emission levels during a
438 saturating pulse and in the dark, respectively. NPQ was calculated as $(F_m - F_m')/F_m'$ (Bilger
439 and Björkman, 1990), where F_m' is the maximum fluorescence emission level in cells
440 exposed to actinic light, measured with the saturating pulse of light. The maximal NPQ
441 response was measured upon exposure for 10 minutes to saturating $950 \mu\text{mol m}^{-2}\cdot\text{s}^{-1}$ green
442 light. Photoinactivation was determined as $(1/F_o - 1/F_m)$ (Park et al., 1995; He and Chow,
443 2003; Wu et al., 2011; Campbell and Tyystjärvi, 2012). Here, the value $(1/F_o - 1/F_m)$ of LL-
444 acclimated or two days of HL-acclimated cells was taken before starting a short HL treatment
445 ($950 \mu\text{mol m}^{-2}\cdot\text{s}^{-1}$) and was set to 100%. The percentage of functional PSII was estimated by
446 calculating $(1/F_o - 1/F_m)$ after the 10-min HL treatment and 15 min of darkness.

447 **Low temperature time-resolved fluorescence emission spectra measurements using a**
448 **streak-camera:** Time-resolved emission spectra were recorded using a synchroscan streak-
449 camera system as described (van Oort et al., 2009). An excitation wavelength of 540 nm was
450 used to preferentially excite fucoxanthin (FX) in the antenna, while 400 nm was used to
451 preferentially excite chlorophyll *a* (Chl *a*) in the antenna and the cores. All samples were

452 measured in two different states: the original (“unq”) state (10 min of dark adaptation) and
453 the “quenched” state (~10 min of preillumination with white light at ~400 $\mu\text{mol photons m}^{-2}$
454 s^{-1}). The laser power was 40-60 μW , the time-window was 2 ns, the spot size was 100 μm ,
455 and the repetition rate was 250 kHz. An average of 100 images, all measured for 10 s, was
456 used to achieve a high signal/noise ratio. Before analysis, the images were corrected for
457 background signal and detector sensitivity and sliced into traces of 5 nm. The streak-camera
458 images were analyzed as described previously (Chukhutsina et al., 2013) with a singular-
459 value-decomposition (SVD) algorithm (van Stokkum et al., 2004). In short, the total dataset
460 was fitted with the function $f(t, \lambda)$:

$$f(t, \lambda) = \sum_{1,2,\dots}^N \text{DAS}_i(\lambda) \exp\left(-\frac{t}{\tau_i}\right) \oplus i(t)$$

461 where DAS (decay-associated spectra) are the wavelength-dependent amplitude factors
462 associated with decay component i having a decay lifetime τ_i (van Stokkum et al., 2004). The
463 number of significant decay components was determined by the SVD algorithm analysis of
464 the data and was 5 for LL and 4 for HL. A Gaussian-shaped instrument response function
465 ($i(t)$) was used as input for the analysis with the width as a free-fitting parameter. The full
466 width at half maximum (FWHM) values of this function, obtained from the fitting procedure,
467 were in the range of 28 ± 2 ps. The slowest component was always fixed to 4 ns. Due to the
468 limited time window of our setup, it was not possible to resolve this component in an
469 accurate way, but for the presented analysis the exact value is not important. When we add
470 all 5 DAS for a specific sample and excitation wavelength, then we obtain the fluorescence
471 spectrum immediately after excitation ($t=0$) before any spectral evolution has taken place in
472 the corresponding wavelength region (unless some processes are too fast to be detected).
473 This can be derived by filling in $t=0$ in the equation above, which leads to $\exp(-t/\tau_i) = 1$ for all

474 values of i . The resulting $t=0$ spectra (before the fluorescence decays sets in) do not depend
475 on the state of the cells (unquenched/quenched), as expected. For comparison of
476 fluorescence emission in quenched and unquenched states (Fig. 5), the total fluorescence
477 spectra at $t = 0$ are normalized to their maximum, while the DAS are scaled accordingly.
478 These scaled DAS were also used to reconstruct the steady-state fluorescence spectra by
479 multiplying the individual, scaled DAS with their corresponding lifetime and taking their
480 weighted sum.

481 **Accession Numbers**

482 Sequence data from this article can be found on the *P. tricornutum* genome browser
483 (annotation Phatr3) on the Ensembl portal
484 (http://protists.ensembl.org/Phaeodactylum_tricornutum/Info/Index) under the following
485 ID numbers: LHCX1: Phatr3_J27278; LHCX2 Phatr3_EG02404; LHCX3: Phatr3_J44733; LHCX4
486 Phatr3_J38720.

487

488 **Supplemental Data**

489 **Supplemental Figure 1:** Representative fluorescence traces used to calculate NPQ values
490 in Figure 1.

491 **Supplemental Figure 2:** Growth rate analysis of wild-type (WT) and LHCX1 knock-down
492 (*lhcx1*) lines after a low light (LL) to high light (HL) shift.

493 **Supplemental Table 1.** Pigment composition of *P. tricornutum* wild-type (WT) and *lhcx1*
494 knock-down lines grown either in low (LL) or high light (HL) for two days.

495 **Supplemental Table 2.** Results of global fitting of the streak-camera data upon 400 nm
496 and 540 nm excitation in unquenched (unq) and quenched (q) states.

497 **Supplemental Table 3.** Calculated averaged lifetimes at characteristic wavelengths in *P.*
498 *tricornutum* wild-type (WT) and *lhcx1* line grown in low light (LL) or high light (HL).

499 **Supplemental Table 4.** Photosystem II efficiency in wild type (WT) and *lhcx1* lines.

500 **Figure Legends**

501 **Figure 1.** *LHCX1* knock-down cells recover their NPQ capacity during prolonged HL exposure.
502 For all the experiments shown in this figure, cells were grown in 12-h-light/12-h-dark cycles
503 either in low light (LL) (30 $\mu\text{mol photons m}^{-2} \text{s}^{-1}$) or in high light (HL) (500 $\mu\text{mol photons m}^{-2}$
504 s^{-1}) for 2 days, following a shift from LL to HL. The samples were taken 2 hours after the
505 onset of light. A and B, NPQ capacity in *P. tricornutum* wild-type (WT, black) and *LHCX1*
506 knock-down (*lhcx1*, white) cells grown under LL (A) or HL (B). Note that different vertical
507 axes were used in panels (A) and (B) to better highlight the differences in NPQ between WT
508 and *lhcx1* cells in LL and HL conditions. Bars indicate +/- standard deviation of five
509 independent experiments. C and D, Accumulation of the different *P. tricornutum* LHCX
510 proteins in WT and *lhcx1* cells detected with an antibody against LHCSR/LHCX. Thirty
511 micrograms from each protein extract were used, and the protein levels were quantified
512 using a serial dilution of proteins from wild-type cells as standard. The relative amount of
513 protein loaded on the gel and the three detected *P. tricornutum* LHCX isoforms (Taddei et
514 al., 2016) are indicated. βCF1 was used as a loading control. The longer exposure time of the
515 membrane in D allowed us to detect the accumulation of the LHCX2 isoform in HL. The
516 vertical lines indicate non-adjacent lanes taken from the same blot. E, Analysis of the relative
517 transcript levels of *LHCX* by RT-qPCR in WT and *lhcx1* cells. The *RPS* (ribosomal protein small
518 subunit 30S; Phatr3_J10847) was used as a reference gene, and for each LHCX, the values
519 are relative to the WT level in LL. Bars represent +/- SD of 3 technical replicates.

520 **Figure 2.** Localization of the LHCX isoforms in different chloroplast fractions. A, Sucrose
521 density gradient fractionation of solubilized thylakoids from wild-type (WT) and *lhcx1* cells
522 grown in LL and in HL for two days. FP, free pigments; FCP, fucoxanthin chlorophyll binding
523 protein complex; PSI, photosystem I; PSII m, photosystem II monomers; PSII d, PSII dimers. B,
524 Western blot analysis of the proteins extracted from the thylakoids and the FCP, PSII, and PSI
525 fractions and detected with antibodies against LHCSR/LHCX, LHCF (antenna proteins), D2
526 (PSII), and PsaF (PSI). Grey panels represent no signal detected after hybridization with the
527 indicated antibodies. Samples were loaded at an equal chlorophyll amount (1 μg). CBB,
528 Coomassie Brilliant Blue staining of the protein gels.

529 **Figure 3.** Time-resolved fluorescence analysis of *P. tricornutum* cells adapted to low light. A
530 and B, Decay-associated spectra (DAS) for wild-type (WT) cells upon a 400-nm excitation (A)
531 and a 540-nm excitation (B) in unquenched (unq, solid lines) and quenched (q, dotted lines)
532 states. C and D, DAS for *lhcx1* cells upon a 400-nm excitation (C) and a 540-nm excitation (D)
533 in unquenched (unq, solid lines) and quenched (q, dotted lines) states. Measurements were
534 performed at 77 Kelvin. DAS were calculated as explained in methods.

535 **Figure 4.** Time-resolved fluorescence analysis of *P. tricornutum* cells adapted to high light. A
536 and B, Decay-associated spectra (DAS) for wild-type (WT) cells upon a 400-nm excitation (A)
537 and a 540-nm excitation (B) in unquenched (unq, solid lines) and quenched (q, dotted lines)
538 states. C and D, DAS for *lhcx1* cells upon a 400-nm excitation (C) and a 540-nm excitation (D)
539 in unquenched (unq, solid lines) and quenched (q, dotted lines) states. Measurements were
540 performed at 77 K. DAS were calculated as explained in methods.

541 **Figure 5.** Reconstructed steady-state emission spectra in unquenched (solid line) and
542 quenched (dashed line) states at 77 K of LL-adapted (first row) and HL-adapted (second row)

543 cells. Excitation wavelengths and analysed strains are indicated in every figure panel. Spectra
544 were reconstructed as explained in methods.

545 **Figure 6.** Physiological analysis of wild-type (WT) and *lhcx1* cells. A and B, Net photosynthesis
546 calculated from the oxygen evolution rates minus oxygen consumption measured with a
547 Clark electrode at different light intensities (0, 90, 200, 450, 750, and 2300 $\mu\text{mol photons m}^{-2}$
548 s^{-1}). WT (A) and *lhcx1* (B) cells were grown in low light (LL, 30 $\mu\text{mol photons m}^{-2} \text{s}^{-1}$) or high
549 light (HL, 500 $\mu\text{mol photons m}^{-2} \text{s}^{-1}$) for two days, following a shift from LL to HL. Bars
550 indicate the standard deviation of three biological replicates. C, Western blot analysis of
551 total protein extracts (30 μg) from cells grown in the same condition as in A and B.
552 Antibodies against LHCSR/LHCX, LHCF, D2, PsaF, and βCF1 were used for protein detection.
553 D, Densitometric analysis of D2 and PsaF obtained from independent western blot analyses
554 (three independent biological experiments) from WT and *lhcx1* cells grown as in (C). Signals
555 for D2 and PsaF were adjusted according to those of βCF1 , used as loading control, and
556 normalized on the WT LL signal.

557 **Figure 7.** Model for NPQ in *P. tricornutum* wild-type (WT) and *lhcx1* cells adapted to low light
558 (LL) and after short and long exposures to high light (HL). In LL-grown WT cells experiencing a
559 short HL-treatment (from seconds to minutes), the major quenching site is close to the
560 reaction centre (PSII QS, Q2). *lhcx1* cells show a reduced quenching capacity because of the
561 reduced content of LHCX1, the highly expressed isoform in LL. After prolonged HL treatment
562 (days), the quenching sites are mainly in the FCP red-shifted antenna (Antenna QS, Q1). The
563 *lhcx1* line recovers its NPQ capacity. Because of the similar quenching capacity in WT and
564 *lhcx1* cells, this quenching could be related to LHCX3, which is highly induced in HL and is
565 detected in the FCP fraction.

566

- 568 **Alboresi A, Gerotto C, Giacometti GM, Bassi R, Morosinotto T** (2010) Physcomitrella patens
569 mutants affected on heat dissipation clarify the evolution of photoprotection mechanisms
570 upon land colonization. *Proc Natl Acad Sci* **107**: 11128–11133
- 571 **Alipanah L, Rohloff J, Winge P, Bones AM, Brembu T** (2015) Whole-cell response to nitrogen
572 deprivation in the diatom *Phaeodactylum tricornutum*. *J Exp Bot* **66**: 6281–6296
- 573 **Allen AE, Dupont CL, Oborník M, Horák A, Nunes-Nesi A, McCrow JP, Zheng H, Johnson DA,**
574 **Hu H, Fernie AR, et al** (2011) Evolution and metabolic significance of the urea cycle in
575 photosynthetic diatoms. *Nature* **473**: 203–207
- 576 **Allen AE, LaRoche J, Maheswari U, Lommer M, Schauer N, Lopez PJ, Finazzi G, Fernie AR,**
577 **Bowler C** (2008) Whole-cell response of the pennate diatom *Phaeodactylum tricornutum* to
578 iron starvation. *Proc Natl Acad Sci* **105**: 10438–10443
- 579 **Allorent G, Tokutsu R, Roach T, Peers G, Cardol P, Girard-Bascou J, Seigneurin-Berny D,**
580 **Petroutsos D, Kuntz M, Breyton C, et al** (2013) A Dual Strategy to Cope with High Light in
581 *Chlamydomonas reinhardtii*. *Plant Cell* **25**: 545–557
- 582 **Bailleul B, Berne N, Murik O, Petroutsos D, Prihoda J, Tanaka A, Villanova V, Bligny R, Flori**
583 **S, Falconet D, et al** (2015) Energetic coupling between plastids and mitochondria drives CO₂
584 assimilation in diatoms. *Nature* **524**: 366–369
- 585 **Bailleul B, Rogato A, de Martino A, Coesel S, Cardol P, Bowler C, Falciatore A, Finazzi G**
586 (2010) An atypical member of the light-harvesting complex stress-related protein family
587 modulates diatom responses to light. *Proc Natl Acad Sci U S A* **107**: 18214–18219
- 588 **Ballottari M, Truong TB, De Re E, Erickson E, Stella GR, Fleming GR, Bassi R, Niyogi KK**
589 (2016) Identification of pH-sensing Sites in the Light Harvesting Complex Stress-related 3
590 Protein Essential for Triggering Non-photochemical Quenching in *Chlamydomonas*
591 *reinhardtii*. *J Biol Chem* **291**: 7334–7346
- 592 **Bergantino E, Segalla A, Brunetta A, Teardo E, Rigoni F, Giacometti GM, Szabò I** (2003)
593 Light- and pH-dependent structural changes in the PsbS subunit of photosystem II. *Proc Natl*
594 *Acad Sci U S A* **100**: 15265–15270
- 595 **Bilger W, Björkman O** (1990) Role of the xanthophyll cycle in photoprotection elucidated by
596 measurements of light-induced absorbance changes, fluorescence and photosynthesis in
597 leaves of *Hedera canariensis*. *Photosynth Res* **25**: 173–185
- 598 **Bonente G, Formighieri C, Mantelli M, Catalanotti C, Giuliano G, Morosinotto T, Bassi R**
599 (2011) Mutagenesis and phenotypic selection as a strategy toward domestication of
600 *Chlamydomonas reinhardtii* strains for improved performance in photobioreactors.
601 *Photosynth Res* **108**: 107–120
- 602 **Campbell DA, Tyystjärvi E** (2012) Parameterization of photosystem II photoinactivation and
603 repair. *Biochim Biophys Acta BBA - Bioenerg* **1817**: 258–265
- 604 **Chukhutsina V, Bersanini L, Aro E-M, van Amerongen H** (2015) Cyanobacterial Light-
605 Harvesting Phycobilisomes Uncouple From Photosystem I During Dark-To-Light Transitions.
606 *Sci Rep* **5**: 14193
- 607 **Chukhutsina VU, Büchel C, van Amerongen H** (2014) Disentangling two non-photochemical
608 quenching processes in *Cyclotella meneghiniana* by spectrally-resolved picosecond
609 fluorescence at 77K. *Biochim Biophys Acta BBA - Bioenerg* **1837**: 899–907
- 610 **Chukhutsina VU, Büchel C, van Amerongen H** (2013) Variations in the first steps of
611 photosynthesis for the diatom *Cyclotella meneghiniana* grown under different light
612 conditions. *Biochim Biophys Acta BBA - Bioenerg* **1827**: 10–18

613 **Dall'Osto L, Cazzaniga S, Bressan M, Paleček D, Židek K, Niyogi KK, Fleming GR, Zigmantas**
614 **D, Bassi R** (2017) Two mechanisms for dissipation of excess light in monomeric and trimeric
615 light-harvesting complexes. *Nat Plants* **3**: 17033

616 **Eberhard S, Finazzi G, Wollman F-A** (2008) The dynamics of photosynthesis. *Annu Rev Genet*
617 **42**: 463–515

618 **Falkowski PG, Owens TG** (1980) Light-Shade Adaptation : TWO STRATEGIES IN MARINE
619 PHYTOPLANKTON. *Plant Physiol* **66**: 592–595

620 **Fan M, Li M, Liu Z, Cao P, Pan X, Zhang H, Zhao X, Zhang J, Chang W** (2015) Crystal
621 structures of the PsbS protein essential for photoprotection in plants. *Nat Struct Mol Biol* **22**:
622 729–735

623 **Gardian Z, Litvín R, Bína D, Vácha F** (2014) Supramolecular organization of fucoxanthin–
624 chlorophyll proteins in centric and pennate diatoms. *Photosynth Res* **121**: 79–86

625 **Ghazaryan A, Akhtar P, Garab G, Lambrev PH, Büchel C** (2016) Involvement of the Lhcx
626 protein Fcp6 of the diatom *Cyclotella meneghiniana* in the macro-organisation and structural
627 flexibility of thylakoid membranes. *Biochim Biophys Acta BBA - Bioenerg* **1857**: 1373–1379

628 **Giovagnetti V, Ruban AV** (2017) Detachment of the fucoxanthin chlorophyll a/c binding
629 protein (FCP) antenna is not involved in the acclimative regulation of photoprotection in the
630 pennate diatom *Phaeodactylum tricornutum*. *Biochim Biophys Acta BBA - Bioenerg* **1858**:
631 218–230

632 **Grouneva I, Rokka A, Aro E-M** (2011) The thylakoid membrane proteome of two marine
633 diatoms outlines both diatom-specific and species-specific features of the photosynthetic
634 machinery. *J Proteome Res* **10**: 5338–5353

635 **He J, Chow WS** (2003) The rate coefficient of repair of photosystem II after
636 photoinactivation. *Physiol Plant* **118**: 297–304

637 **Herbstová M, Bína D, Kaňa R, Vácha F, Litvín R** (2017) Red-light phenotype in a marine
638 diatom involves a specialized oligomeric red-shifted antenna and altered cell morphology.
639 *Sci Rep* **7**: 11976

640 **Herbstová M, Bína D, Koník P, Gardian Z, Vácha F, Litvín R** (2015) Molecular basis of
641 chromatic adaptation in pennate diatom *Phaeodactylum tricornutum*. *Biochim Biophys Acta*
642 *BBA - Bioenerg* **1847**: 534–543

643 **Horton P, Ruban AV, Walters RG** (1996) REGULATION OF LIGHT HARVESTING IN GREEN
644 PLANTS. *Annu Rev Plant Physiol Plant Mol Biol* **47**: 655–684

645 **Johnson X, Vandystadt G, Bujaldon S, Wollman F-A, Dubois R, Roussel P, Alric J, Béal D**
646 (2009) A new setup for in vivo fluorescence imaging of photosynthetic activity. *Photosynth*
647 *Res* **102**: 85–93

648 **Joshi-Deo J, Schmidt M, Gruber A, Weisheit W, Mittag M, Kroth PG, Büchel C** (2010)
649 Characterization of a trimeric light-harvesting complex in the diatom *Phaeodactylum*
650 *tricornutum* built of FcpA and FcpE proteins. *J Exp Bot* **61**: 3079–3087

651 **Kuzminov FI, Gorbunov MY** (2016) Energy dissipation pathways in Photosystem 2 of the
652 diatom, *Phaeodactylum tricornutum*, under high-light conditions. *Photosynth Res* **127**: 219–
653 235

654 **Lepetit B, Gélín G, Lepetit M, Sturm S, Vugrinec S, Rogato A, Kroth PG, Falciatore A, Lavaud**
655 **J** (2017) The diatom *Phaeodactylum tricornutum* adjusts nonphotochemical fluorescence
656 quenching capacity in response to dynamic light via fine-tuned Lhcx and xanthophyll cycle
657 pigment synthesis. *New Phytol* **214**: 205–218

658 **Lepetit B, Sturm S, Rogato A, Gruber A, Sachse M, Falciatore A, Kroth PG, Lavaud J** (2013)
659 High Light Acclimation in the Secondary Plastids Containing Diatom *Phaeodactylum*

660 tricornutum is Triggered by the Redox State of the Plastoquinone Pool. *PLANT Physiol* **161**:
661 853–865

662 **Lepetit B, Volke D, Gilbert M, Wilhelm C, Goss R** (2010) Evidence for the Existence of One
663 Antenna-Associated, Lipid-Dissolved and Two Protein-Bound Pools of Diadinoxanthin Cycle
664 Pigments in Diatoms. *PLANT Physiol* **154**: 1905–1920

665 **Lepetit B, Volke D, Szabó M, Hoffmann R, Garab G, Wilhelm C, Goss R** (2007) Spectroscopic
666 and molecular characterization of the oligomeric antenna of the diatom *Phaeodactylum*
667 *tricornutum*. *Biochemistry (Mosc)* **46**: 9813–9822

668 **Lohr M, Wilhelm C** (1999) Algae displaying the diadinoxanthin cycle also possess the
669 violaxanthin cycle. *Proc Natl Acad Sci U S A* **96**: 8784–8789

670 **Lohr M, Wilhelm C** (2001) Xanthophyll synthesis in diatoms: quantification of putative
671 intermediates and comparison of pigment conversion kinetics with rate constants derived
672 from a model. *Planta* **212**: 382–391

673 **Malviya S, Scalco E, Audic S, Vincent F, Veluchamy A, Poulain J, Wincker P, Iudicone D, de**
674 **Vargas C, Bittner L, et al** (2016) Insights into global diatom distribution and diversity in the
675 world's ocean. *Proc Natl Acad Sci* **113**: E1516–E1525

676 **Marchetti A, Schruth DM, Durkin CA, Parker MS, Kodner RB, Berthiaume CT, Morales R,**
677 **Allen AE, Armbrust EV** (2012) Comparative metatranscriptomics identifies molecular bases
678 for the physiological responses of phytoplankton to varying iron availability. *Proc Natl Acad*
679 *Sci* **109**: E317–E325

680 **Matthijs M, Fabris M, Broos S, Vyverman W, Goossens A** (2016) Profiling of the Early
681 Nitrogen Stress Response in the Diatom *Phaeodactylum tricornutum* Reveals a Novel Family
682 of RING-Domain Transcription Factors. *Plant Physiol* **170**: 489–498

683 **McQuaid JB, Kustka AB, Oborník M, Horák A, McCrow JP, Karas BJ, Zheng H, Kindeberg T,**
684 **Andersson AJ, Barbeau KA, et al** (2018) Carbonate-sensitive phytoferritin controls high-
685 affinity iron uptake in diatoms. *Nature* **555**: 534–537

686 **Miloslavina Y, Grouneva I, Lambrev PH, Lepetit B, Goss R, Wilhelm C, Holzwarth AR** (2009)
687 Ultrafast fluorescence study on the location and mechanism of non-photochemical
688 quenching in diatoms. *Biochim Biophys Acta BBA - Bioenerg* **1787**: 1189–1197

689 **Mock T, Otilar RP, Strauss J, McMullan M, Paajanen P, Schmutz J, Salamov A, Sanges R,**
690 **Toseland A, Ward BJ, et al** (2017) Evolutionary genomics of the cold-adapted diatom
691 *Fragilariopsis cylindrus*. *Nature* **541**: 536–540

692 **Morrissey J, Sutak R, Paz-Yepes J, Tanaka A, Moustafa A, Veluchamy A, Thomas Y, Botebol**
693 **H, Bouget F-Y, McQuaid JB, et al** (2015) A Novel Protein, Ubiquitous in Marine
694 Phytoplankton, Concentrates Iron at the Cell Surface and Facilitates Uptake. *Curr Biol* **25**:
695 364–371

696 **Müller P, Li XP, Niyogi KK** (2001) Non-photochemical quenching. A response to excess light
697 energy. *Plant Physiol* **125**: 1558–1566

698 **Nagao R, Takahashi S, Suzuki T, Dohmae N, Nakazato K, Tomo T** (2013) Comparison of
699 oligomeric states and polypeptide compositions of fucoxanthin chlorophyll a/c-binding
700 protein complexes among various diatom species. *Photosynth Res* **117**: 281–288

701 **Nymark M, Valle KC, Brembu T, Hancke K, Winge P, Andresen K, Johnsen G, Bones AM**
702 (2009) An integrated analysis of molecular acclimation to high light in the marine diatom
703 *Phaeodactylum tricornutum*. *PloS One* **4**: e7743

704 **van Oort B, Murali S, Wientjes E, Koehorst RBM, Spruijt RB, van Hoek A, Croce R, van**
705 **Amerongen H** (2009) Ultrafast resonance energy transfer from a site-specifically attached

706 fluorescent chromophore reveals the folding of the N-terminal domain of CP29. *Chem Phys*
707 **357**: 113–119

708 **van Stokkum IHM, Larsen DS, van Grondelle R** (2004) Global and target analysis of time-
709 resolved spectra. *Biochimica et Biophysica Acta (BBA) - Bioenergetics* **1657**: 82–104

710 **van Stokkum IHM, Van Oort B, Van Mourik F, Gobets B, Van Amerongen H** (2008) (Sub)-
711 Picosecond Spectral Evolution of Fluorescence Studied with a Synchroscan Streak-Camera
712 System and Target Analysis. *In* TJ Aartsma, J Matysik, eds, *Biophys. Tech. Photosynth.*
713 Springer Netherlands, Dordrecht, pp 223–240

714 **Park Y-I, Chow W, Anderson J** (1995) Light inactivation of functional photosystem II in leaves
715 of peas grown in moderate light depends on photon exposure. *Planta*. doi:
716 10.1007/BF00203636

717 **Peers G, Truong TB, Ostendorf E, Busch A, Elrad D, Grossman AR, Hippler M, Niyogi KK**
718 (2009) An ancient light-harvesting protein is critical for the regulation of algal
719 photosynthesis. *Nature* **462**: 518–521

720 **Pinnola A, Cazzaniga S, Alboresi A, Nevo R, Levin-Zaidman S, Reich Z, Bassi R** (2015) Light-
721 Harvesting Complex Stress-Related Proteins Catalyze Excess Energy Dissipation in Both
722 Photosystems of *Physcomitrella patens*. *Plant Cell* **27**: 3213–3227

723 **Ruban A, Lavaud J, Rousseau B, Guglielmi G, Horton P, Etienne A-L** (2004) The super-excess
724 energy dissipation in diatom algae: comparative analysis with higher plants. *Photosynth Res*
725 **82**: 165–175

726 **Schaller-Laudel S, Volke D, Redlich M, Kansy M, Hoffmann R, Wilhelm C, Goss R** (2015) The
727 diadinoxanthin diatoxanthin cycle induces structural rearrangements of the isolated FCP
728 antenna complexes of the pennate diatom *Phaeodactylum tricornutum*. *Plant Physiol*
729 *Biochem* **96**: 364–376

730 **Schneider CA, Rasband WS, Eliceiri KW** (2012) NIH Image to ImageJ: 25 years of image
731 analysis. *Nat Methods* **9**: 671–675

732 **Smetacek V** (1999) Diatoms and the Ocean Carbon Cycle. *Protist* **150**: 25–32

733 **Szabó M, Lepetit B, Goss R, Wilhelm C, Mustárdy L, Garab G** (2008) Structurally flexible
734 macro-organization of the pigment–protein complexes of the diatom *Phaeodactylum*
735 *tricornutum*. *Photosynth Res* **95**: 237–245

736 **Taddei L, Stella GR, Rogato A, Bailleul B, Fortunato AE, Annunziata R, Sanges R, Thaler M,**
737 **Lepetit B, Lavaud J, et al** (2016) Multisignal control of expression of the LHCX protein family
738 in the marine diatom *Phaeodactylum tricornutum*. *J Exp Bot* **67**: 3939–3951

739 **Tian L, Xu P, Chukhutsina VU, Holzwarth AR, Croce R** (2017) Zeaxanthin-dependent
740 nonphotochemical quenching does not occur in photosystem I in the higher plant
741 *Arabidopsis thaliana*. *Proc Natl Acad Sci U S A* **114**: 4828–4832

742 **Ünlü C, Polukhina I, van Amerongen H** (2016) Origin of pronounced differences in 77 K
743 fluorescence of the green alga *Chlamydomonas reinhardtii* in state 1 and 2. *Eur Biophys J EBJ*
744 **45**: 209–217

745 **de Vargas C, Audic S, Henry N, Decelle J, Mahe F, Logares R, Lara E, Berney C, Le Bescot N,**
746 **Probert I, et al** (2015) Eukaryotic plankton diversity in the sunlit ocean. *Science* **348**:
747 1261605–1261605

748 **van der Weij-de Wit CD, Dekker JP, van Grondelle R, van Stokkum IHM** (2011) Charge
749 separation is virtually irreversible in photosystem II core complexes with oxidized primary
750 quinone acceptor. *J Phys Chem A* **115**: 3947–3956

751 **Wientjes E, van Stokkum IHM, van Amerongen H, Croce R** (2011) The role of the individual
752 Lhcas in photosystem I excitation energy trapping. *Biophys J* **101**: 745–754

753 **Włodarczyk LM, Dinc E, Croce R, Dekker JP** (2016) Excitation energy transfer in
754 *Chlamydomonas reinhardtii* deficient in the PSI core or the PSII core under conditions
755 mimicking state transitions. *Biochim Biophys Acta* **1857**: 625–633
756 **Wu H, Cockshutt AM, McCarthy A, Campbell DA** (2011) Distinctive Photosystem II
757 Photoinactivation and Protein Dynamics in Marine Diatoms. *PLANT Physiol* **156**: 2184–2195
758 **Zhu S-H, Green BR** (2010) Photoprotection in the diatom *Thalassiosira pseudonana*: Role of
759 LI818-like proteins in response to high light stress. *Biochim Biophys Acta BBA - Bioenerg*
760 **1797**: 1449–1457
761

762

Figure 1 – Taddei et al.

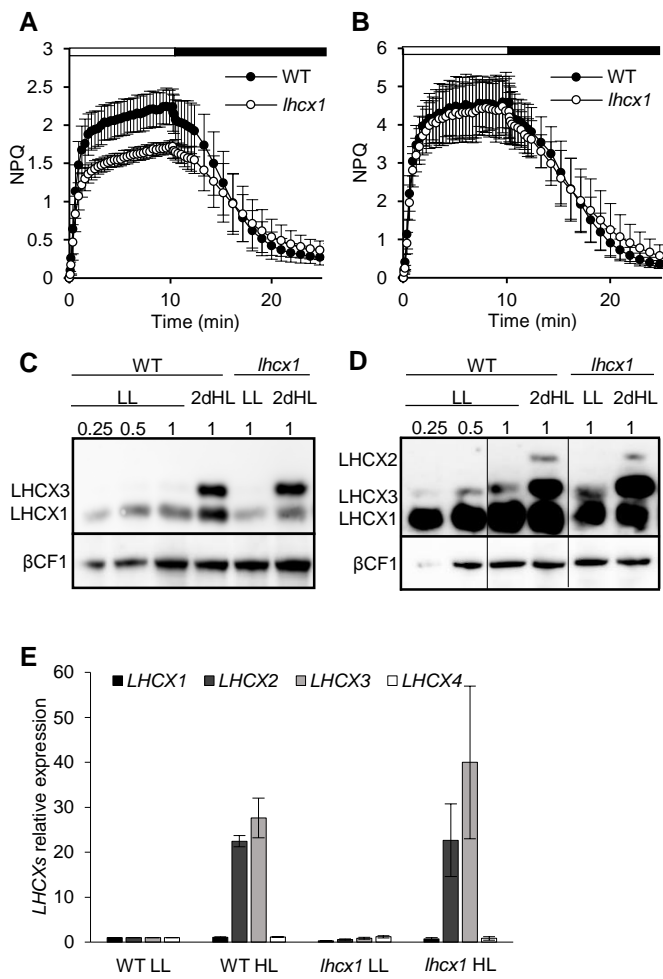


Figure 2 – Taddei et al.

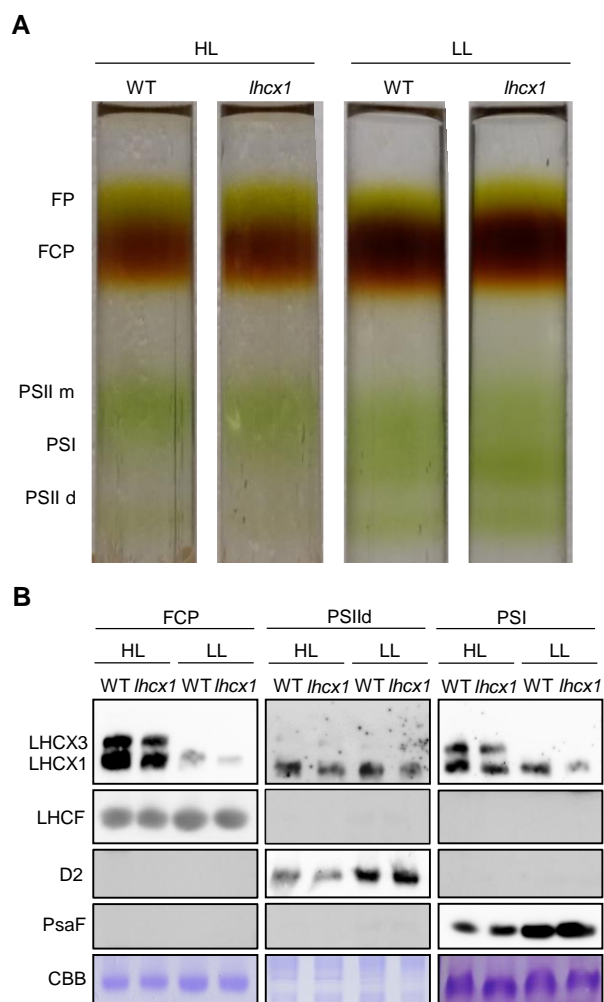


Figure 3 – Taddei et al.

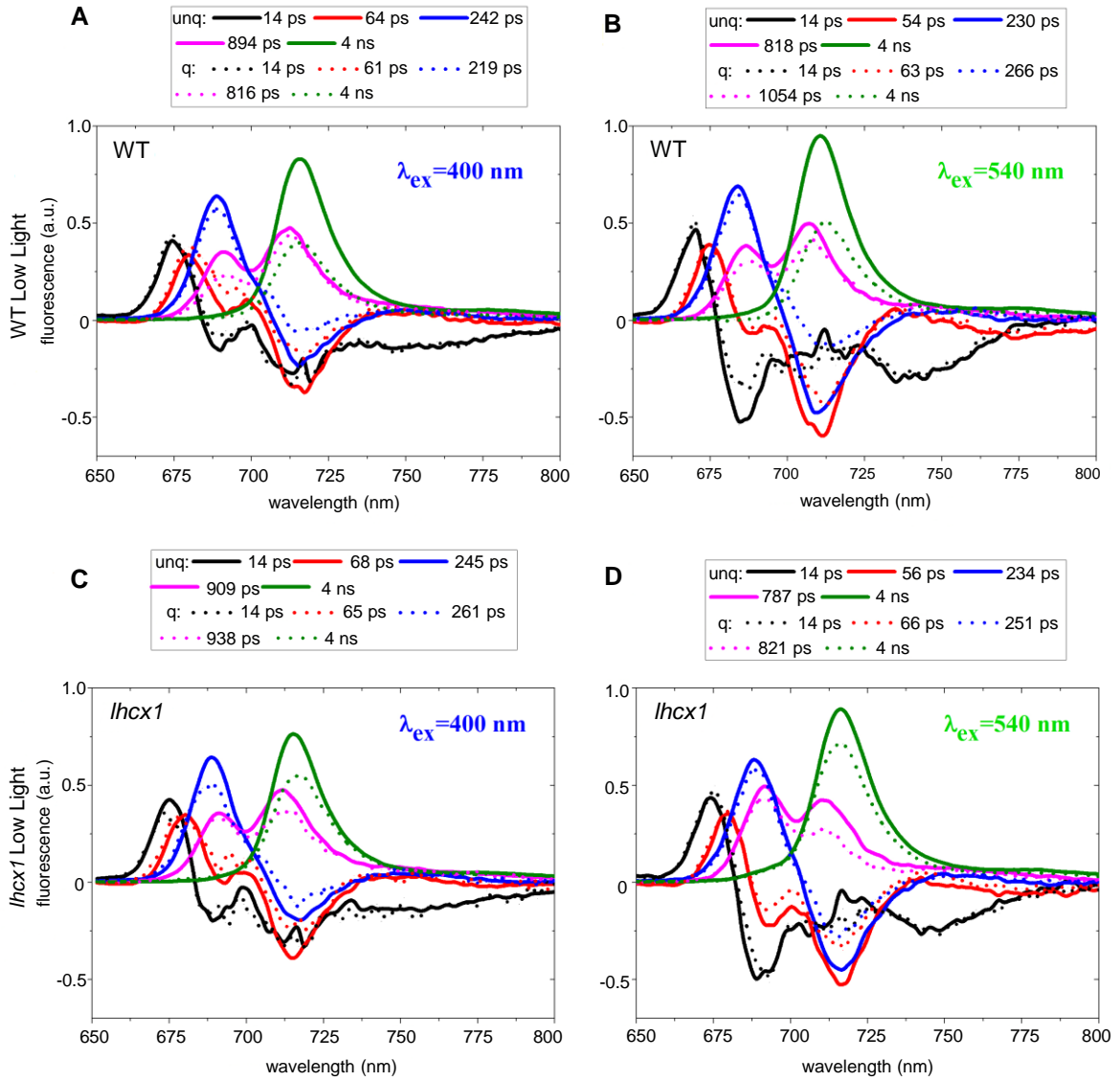
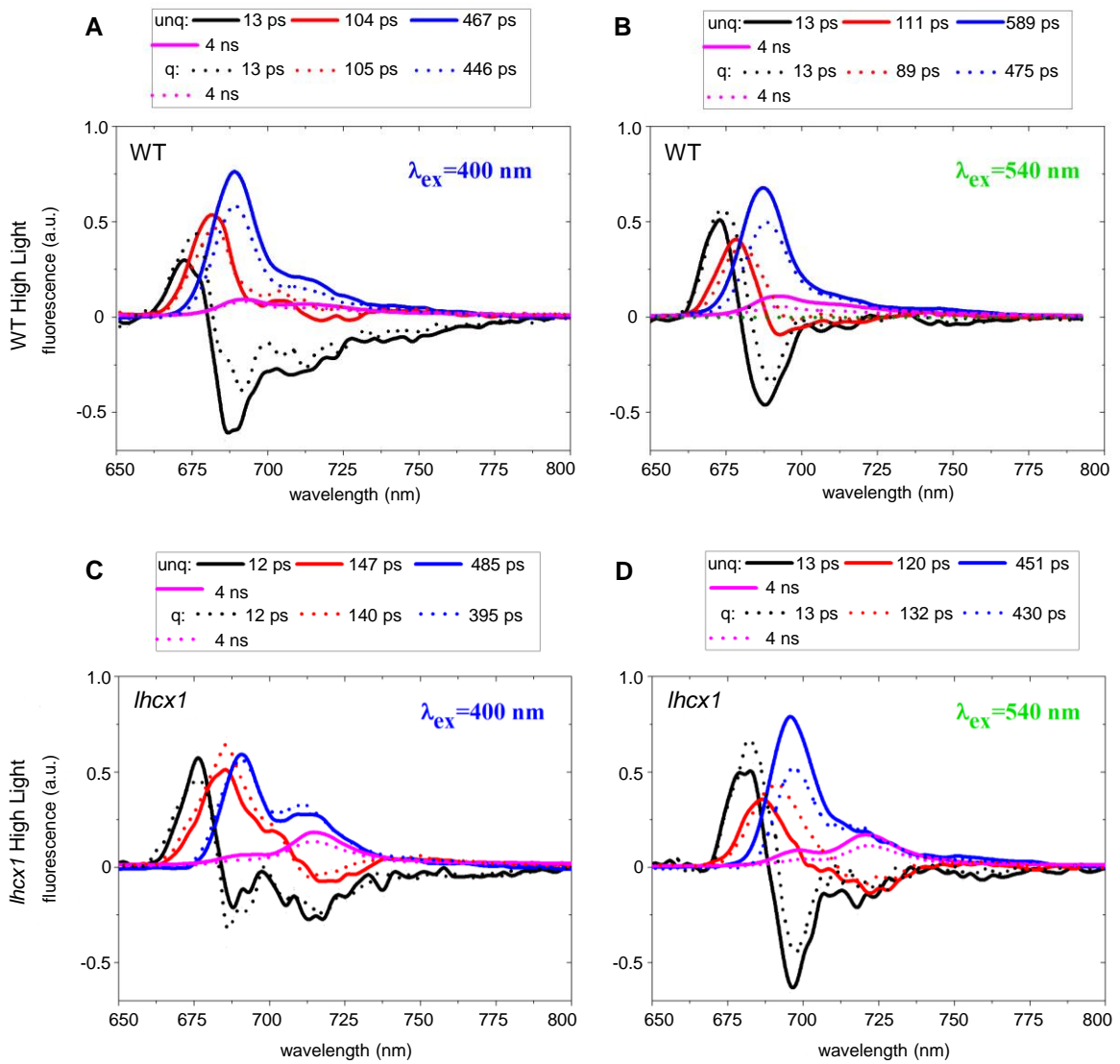


Figure 4 – Taddei et al.



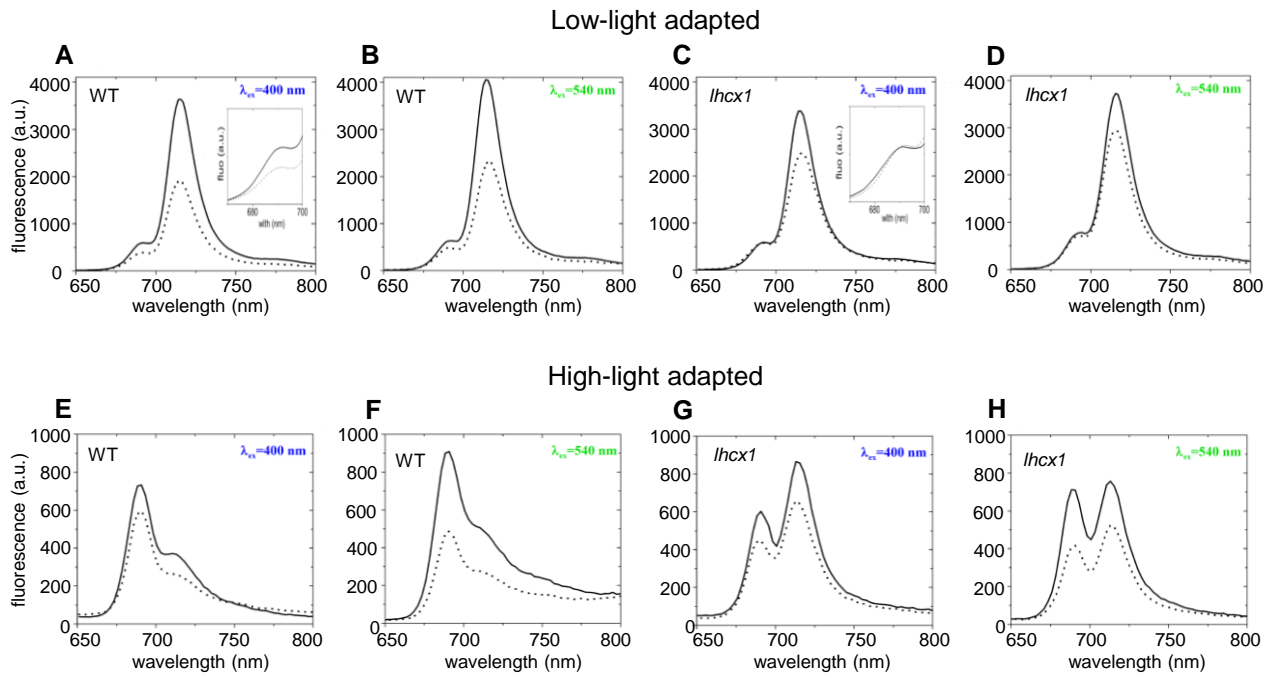


Figure 6 – Taddei et al.

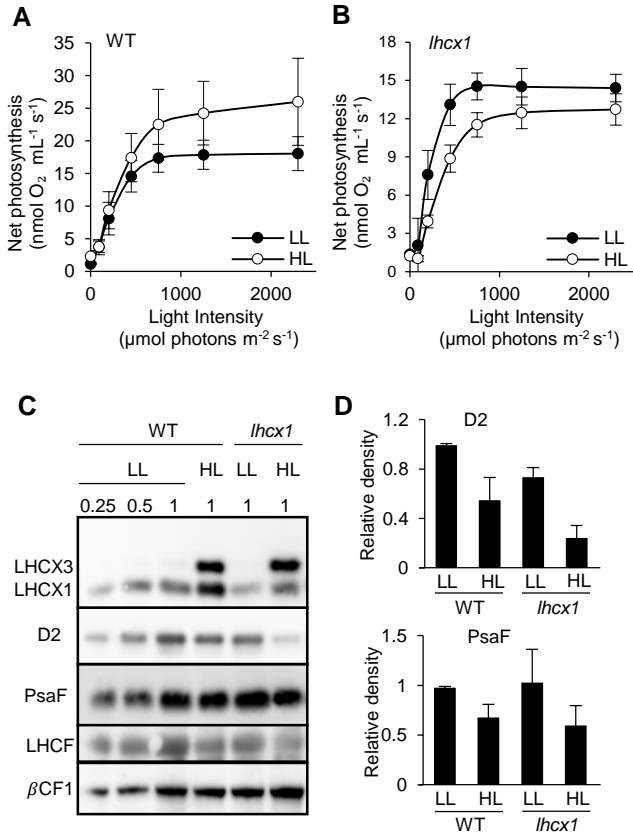
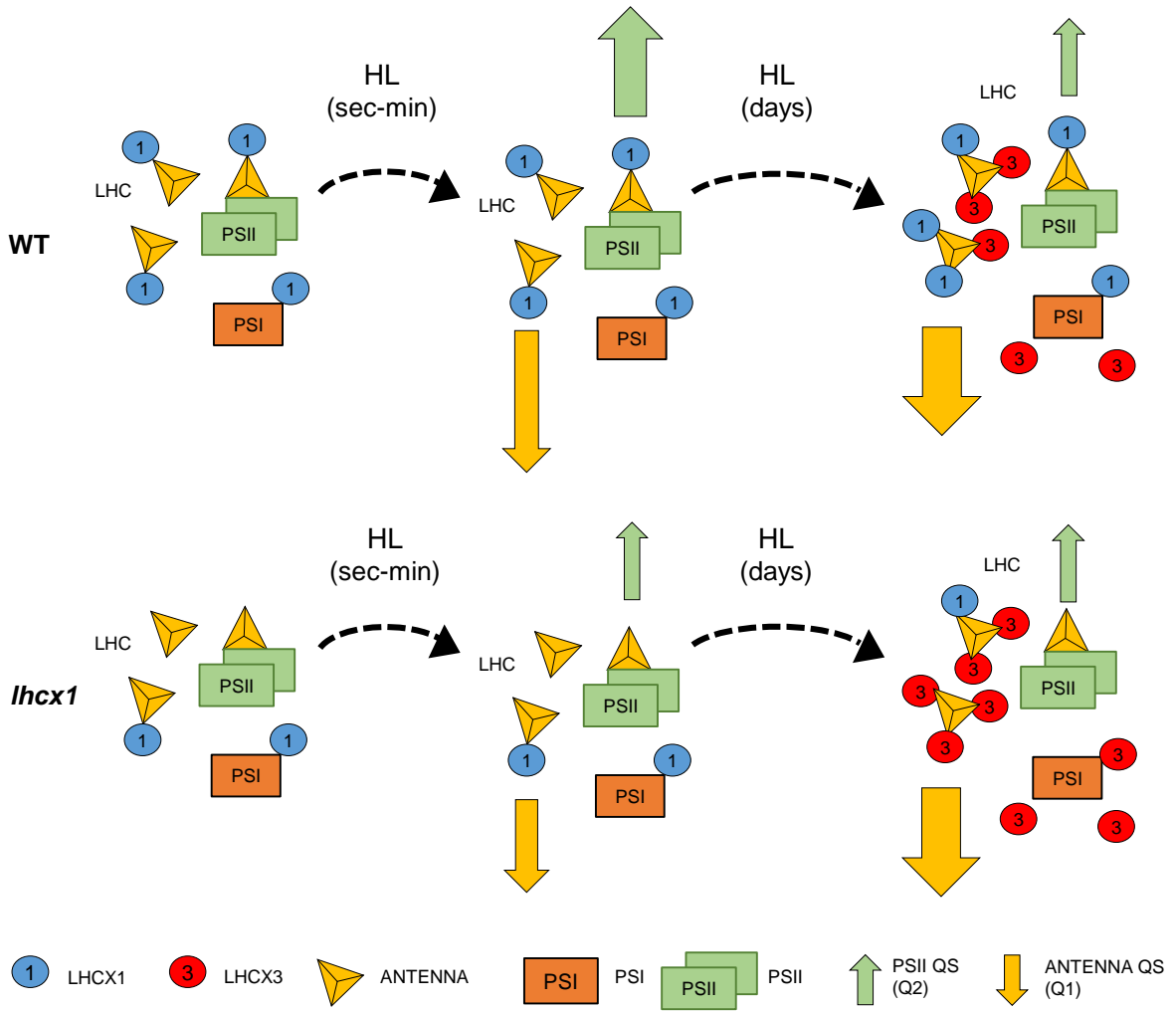


Figure 7 – Taddei et al.



Parsed Citations

Alboresi A, Gerotto C, Giacometti GM, Bassi R, Morosinotto T (2010) Physcomitrella patens mutants affected on heat dissipation clarify the evolution of photoprotection mechanisms upon land colonization. Proc Natl Acad Sci 107: 11128–11133

Pubmed: [Author and Title](#)

CrossRef: [Author and Title](#)

Google Scholar: [Author Only](#) [Title Only](#) [Author and Title](#)

Alipanah L, Rohloff J, Winge P, Bones AM, Brembu T (2015) Whole-cell response to nitrogen deprivation in the diatom Phaeodactylum tricornutum. J Exp Bot 66: 6281–6296

Pubmed: [Author and Title](#)

CrossRef: [Author and Title](#)

Google Scholar: [Author Only](#) [Title Only](#) [Author and Title](#)

Allen AE, Dupont CL, Oborník M, Horák A, Nunes-Nesi A, McCrow JP, Zheng H, Johnson DA, Hu H, Fernie AR, et al (2011) Evolution and metabolic significance of the urea cycle in photosynthetic diatoms. Nature 473: 203–207

Pubmed: [Author and Title](#)

CrossRef: [Author and Title](#)

Google Scholar: [Author Only](#) [Title Only](#) [Author and Title](#)

Allen AE, LaRoche J, Maheswari U, Lommer M, Schauer N, Lopez PJ, Finazzi G, Fernie AR, Bowler C (2008) Whole-cell response of the pennate diatom Phaeodactylum tricornutum to iron starvation. Proc Natl Acad Sci 105: 10438–10443

Pubmed: [Author and Title](#)

CrossRef: [Author and Title](#)

Google Scholar: [Author Only](#) [Title Only](#) [Author and Title](#)

Allorent G, Tokutsu R, Roach T, Peers G, Cardol P, Girard-Bascou J, Seigneurin-Berny D, Petroutsos D, Kuntz M, Breyton C, et al (2013) A Dual Strategy to Cope with High Light in Chlamydomonas reinhardtii. Plant Cell 25: 545–557

Pubmed: [Author and Title](#)

CrossRef: [Author and Title](#)

Google Scholar: [Author Only](#) [Title Only](#) [Author and Title](#)

Bailleul B, Berne N, Murik O, Petroutsos D, Pihoda J, Tanaka A, Villanova V, Bligny R, Flori S, Falconet D, et al (2015) Energetic coupling between plastids and mitochondria drives CO₂ assimilation in diatoms. Nature 524: 366–369

Pubmed: [Author and Title](#)

CrossRef: [Author and Title](#)

Google Scholar: [Author Only](#) [Title Only](#) [Author and Title](#)

Bailleul B, Rogato A, de Martino A, Coesel S, Cardol P, Bowler C, Falcatore A, Finazzi G (2010) An atypical member of the light-harvesting complex stress-related protein family modulates diatom responses to light. Proc Natl Acad Sci U S A 107: 18214–18219

Pubmed: [Author and Title](#)

CrossRef: [Author and Title](#)

Google Scholar: [Author Only](#) [Title Only](#) [Author and Title](#)

Ballottari M, Truong TB, De Re E, Erickson E, Stella GR, Fleming GR, Bassi R, Niyogi KK (2016) Identification of pH-sensing Sites in the Light Harvesting Complex Stress-related 3 Protein Essential for Triggering Non-photochemical Quenching in Chlamydomonas reinhardtii. J Biol Chem 291: 7334–7346

Pubmed: [Author and Title](#)

CrossRef: [Author and Title](#)

Google Scholar: [Author Only](#) [Title Only](#) [Author and Title](#)

Bergantino E, Segalla A, Brunetta A, Teardo E, Rigoni F, Giacometti GM, Szabó I (2003) Light- and pH-dependent structural changes in the PsbS subunit of photosystem II. Proc Natl Acad Sci U S A 100: 15265–15270

Pubmed: [Author and Title](#)

CrossRef: [Author and Title](#)

Google Scholar: [Author Only](#) [Title Only](#) [Author and Title](#)

Bilger W, Björkman O (1990) Role of the xanthophyll cycle in photoprotection elucidated by measurements of light-induced absorbance changes, fluorescence and photosynthesis in leaves of Hedera canariensis. Photosynth Res 25: 173–185

Pubmed: [Author and Title](#)

CrossRef: [Author and Title](#)

Google Scholar: [Author Only](#) [Title Only](#) [Author and Title](#)

Bonente G, Formighieri C, Mantelli M, Catalanotti C, Giuliano G, Morosinotto T, Bassi R (2011) Mutagenesis and phenotypic selection as a strategy toward domestication of Chlamydomonas reinhardtii strains for improved performance in photobioreactors. Photosynth Res 108: 107–120

Pubmed: [Author and Title](#)

CrossRef: [Author and Title](#)

Google Scholar: [Author Only](#) [Title Only](#) [Author and Title](#)

Campbell DA, Tyystjärvi E (2012) Parameterization of photosystem II photoinactivation and repair. Biochim Biophys Acta BBA - Bioenerg 1817: 258–265

Pubmed: [Author and Title](#)

CrossRef: [Author and Title](#)

Google Scholar: [Author Only](#) [Title Only](#) [Author and Title](#)

Chukhutsina V, Bersanini L, Aro E-M, van Amerongen H (2015) Cyanobacterial Light-Harvesting Phycobilisomes Uncouple From Photosystem I During Dark-To-Light Transitions. Sci Rep 5: 14193

Pubmed: [Author and Title](#)

CrossRef: [Author and Title](#)

Google Scholar: [Author Only](#) [Title Only](#) [Author and Title](#)

Chukhutsina VU, Büchel C, van Amerongen H (2014) Disentangling two non-photochemical quenching processes in *Cyclotella meneghiniana* by spectrally-resolved picosecond fluorescence at 77K. Biochim Biophys Acta BBA - Bioenerg 1837: 899–907

Pubmed: [Author and Title](#)

CrossRef: [Author and Title](#)

Google Scholar: [Author Only](#) [Title Only](#) [Author and Title](#)

Chukhutsina VU, Büchel C, van Amerongen H (2013) Variations in the first steps of photosynthesis for the diatom *Cyclotella meneghiniana* grown under different light conditions. Biochim Biophys Acta BBA - Bioenerg 1827: 10–18

Pubmed: [Author and Title](#)

CrossRef: [Author and Title](#)

Google Scholar: [Author Only](#) [Title Only](#) [Author and Title](#)

Dall'Osto L, Cazzaniga S, Bressan M, Paleček D, Židek K, Niyogi KK, Fleming GR, Zigmantas D, Bassi R (2017) Two mechanisms for dissipation of excess light in monomeric and trimeric light-harvesting complexes. Nat Plants 3: 17033

Pubmed: [Author and Title](#)

CrossRef: [Author and Title](#)

Google Scholar: [Author Only](#) [Title Only](#) [Author and Title](#)

Eberhard S, Finazzi G, Wollman F-A (2008) The dynamics of photosynthesis. Annu Rev Genet 42: 463–515

Pubmed: [Author and Title](#)

CrossRef: [Author and Title](#)

Google Scholar: [Author Only](#) [Title Only](#) [Author and Title](#)

Falkowski PG, Owens TG (1980) Light-Shade Adaptation : TWO STRATEGIES IN MARINE PHYTOPLANKTON. Plant Physiol 66: 592–595

Pubmed: [Author and Title](#)

CrossRef: [Author and Title](#)

Google Scholar: [Author Only](#) [Title Only](#) [Author and Title](#)

Fan M, Li M, Liu Z, Cao P, Pan X, Zhang H, Zhao X, Zhang J, Chang W (2015) Crystal structures of the PsbS protein essential for photoprotection in plants. Nat Struct Mol Biol 22: 729–735

Pubmed: [Author and Title](#)

CrossRef: [Author and Title](#)

Google Scholar: [Author Only](#) [Title Only](#) [Author and Title](#)

Gardian Z, Litvín R, Bína D, Vácha F (2014) Supramolecular organization of fucoxanthin–chlorophyll proteins in centric and pennate diatoms. Photosynth Res 121: 79–86

Pubmed: [Author and Title](#)

CrossRef: [Author and Title](#)

Google Scholar: [Author Only](#) [Title Only](#) [Author and Title](#)

Ghazaryan A, Akhtar P, Garab G, Lambrev PH, Büchel C (2016) Involvement of the Lhcx protein Fcp6 of the diatom *Cyclotella meneghiniana* in the macro-organisation and structural flexibility of thylakoid membranes. Biochim Biophys Acta BBA - Bioenerg 1857: 1373–1379

Pubmed: [Author and Title](#)

CrossRef: [Author and Title](#)

Google Scholar: [Author Only](#) [Title Only](#) [Author and Title](#)

Giovagnetti V, Ruban AV (2017) Detachment of the fucoxanthin chlorophyll a/c binding protein (FCP) antenna is not involved in the acclimative regulation of photoprotection in the pennate diatom *Phaeodactylum tricornutum*. Biochim Biophys Acta BBA - Bioenerg 1858: 218–230

Pubmed: [Author and Title](#)

CrossRef: [Author and Title](#)

Google Scholar: [Author Only](#) [Title Only](#) [Author and Title](#)

Grouneva I, Rokka A, Aro E-M (2011) The thylakoid membrane proteome of two marine diatoms outlines both diatom-specific and species-specific features of the photosynthetic machinery. J Proteome Res 10: 5338–5353

Pubmed: [Author and Title](#)

CrossRef: [Author and Title](#)

Google Scholar: [Author Only](#) [Title Only](#) [Author and Title](#)

He J, Chow WS (2003) The rate coefficient of repair of photosystem II after photoinactivation. Physiol Plant 118: 297–304

Pubmed: [Author and Title](#)

CrossRef: [Author and Title](#)

Google Scholar: [Author Only](#) [Title Only](#) [Author and Title](#)

Herbstová M, Bína D, Kaňa R, Vácha F, Litvín R (2017) Red-light phenotype in a marine diatom involves a specialized oligomeric red-shifted antenna and altered cell morphology. Sci Rep 7: 11976

Pubmed: [Author and Title](#)
CrossRef: [Author and Title](#)
Google Scholar: [Author Only Title Only Author and Title](#)

Herbstová M, Bína D, Koník P, Gardian Z, Vácha F, Litvín R (2015) Molecular basis of chromatic adaptation in pennate diatom *Phaeodactylum tricornutum*. *Biochim Biophys Acta BBA - Bioenerg* 1847: 534–543

Pubmed: [Author and Title](#)
CrossRef: [Author and Title](#)
Google Scholar: [Author Only Title Only Author and Title](#)

Horton P, Ruban AV, Walters RG (1996) REGULATION OF LIGHT HARVESTING IN GREEN PLANTS. *Annu Rev Plant Physiol Plant Mol Biol* 47: 655–684

Pubmed: [Author and Title](#)
CrossRef: [Author and Title](#)
Google Scholar: [Author Only Title Only Author and Title](#)

Johnson X, Vandystadt G, Bujaldon S, Wollman F-A, Dubois R, Roussel P, Alric J, Béal D (2009) A new setup for in vivo fluorescence imaging of photosynthetic activity. *Photosynth Res* 102: 85–93

Pubmed: [Author and Title](#)
CrossRef: [Author and Title](#)
Google Scholar: [Author Only Title Only Author and Title](#)

Joshi-Deo J, Schmidt M, Gruber A, Weisheit W, Mittag M, Kroth PG, Buchel C (2010) Characterization of a trimeric light-harvesting complex in the diatom *Phaeodactylum tricornutum* built of FcpA and FcpE proteins. *J Exp Bot* 61: 3079–3087

Pubmed: [Author and Title](#)
CrossRef: [Author and Title](#)
Google Scholar: [Author Only Title Only Author and Title](#)

Kuzminov FI, Gorbunov MY (2016) Energy dissipation pathways in Photosystem 2 of the diatom, *Phaeodactylum tricornutum*, under high-light conditions. *Photosynth Res* 127: 219–235

Pubmed: [Author and Title](#)
CrossRef: [Author and Title](#)
Google Scholar: [Author Only Title Only Author and Title](#)

Lepetit B, Gélín G, Lepetit M, Sturm S, Vugrinec S, Rogato A, Kroth PG, Falcatore A, Lavaud J (2017) The diatom *Phaeodactylum tricornutum* adjusts nonphotochemical fluorescence quenching capacity in response to dynamic light via fine-tuned Lhcx and xanthophyll cycle pigment synthesis. *New Phytol* 214: 205–218

Pubmed: [Author and Title](#)
CrossRef: [Author and Title](#)
Google Scholar: [Author Only Title Only Author and Title](#)

Lepetit B, Sturm S, Rogato A, Gruber A, Sachse M, Falcatore A, Kroth PG, Lavaud J (2013) High Light Acclimation in the Secondary Plastids Containing Diatom *Phaeodactylum tricornutum* is Triggered by the Redox State of the Plastoquinone Pool. *PLANT Physiol* 161: 853–865

Pubmed: [Author and Title](#)
CrossRef: [Author and Title](#)
Google Scholar: [Author Only Title Only Author and Title](#)

Lepetit B, Volke D, Gilbert M, Wilhelm C, Goss R (2010) Evidence for the Existence of One Antenna-Associated, Lipid-Dissolved and Two Protein-Bound Pools of Diadinoxanthin Cycle Pigments in Diatoms. *PLANT Physiol* 154: 1905–1920

Pubmed: [Author and Title](#)
CrossRef: [Author and Title](#)
Google Scholar: [Author Only Title Only Author and Title](#)

Lepetit B, Volke D, Szabó M, Hoffmann R, Garab G, Wilhelm C, Goss R (2007) Spectroscopic and molecular characterization of the oligomeric antenna of the diatom *Phaeodactylum tricornutum*. *Biochemistry (Mosc)* 46: 9813–9822

Pubmed: [Author and Title](#)
CrossRef: [Author and Title](#)
Google Scholar: [Author Only Title Only Author and Title](#)

Lohr M, Wilhelm C (1999) Algae displaying the diadinoxanthin cycle also possess the violaxanthin cycle. *Proc Natl Acad Sci U S A* 96: 8784–8789

Pubmed: [Author and Title](#)
CrossRef: [Author and Title](#)
Google Scholar: [Author Only Title Only Author and Title](#)

Lohr M, Wilhelm C (2001) Xanthophyll synthesis in diatoms: quantification of putative intermediates and comparison of pigment conversion kinetics with rate constants derived from a model. *Planta* 212: 382–391

Pubmed: [Author and Title](#)
CrossRef: [Author and Title](#)
Google Scholar: [Author Only Title Only Author and Title](#)

Malviya S, Scalco E, Audic S, Vincent F, Veluchamy A, Poulain J, Wincker P, Iudicone D, de Vargas C, Bittner L, et al (2016) Insights into global diatom distribution and diversity in the world's ocean. *Proc Natl Acad Sci* 113: E1516–E1525

Pubmed: [Author and Title](#)

CrossRef: [Author and Title](#)
Google Scholar: [Author Only Title Only Author and Title](#)

Marchetti A, Schrueth DM, Durkin CA, Parker MS, Kodner RB, Berthiaume CT, Morales R, Allen AE, Armbrust EV (2012) Comparative metatranscriptomics identifies molecular bases for the physiological responses of phytoplankton to varying iron availability. Proc Natl Acad Sci 109: E317–E325

Pubmed: [Author and Title](#)
CrossRef: [Author and Title](#)
Google Scholar: [Author Only Title Only Author and Title](#)

Matthijs M, Fabris M, Broos S, Vyverman W, Goossens A (2016) Profiling of the Early Nitrogen Stress Response in the Diatom *Phaeodactylum tricornutum* Reveals a Novel Family of RING-Domain Transcription Factors. Plant Physiol 170: 489–498

Pubmed: [Author and Title](#)
CrossRef: [Author and Title](#)
Google Scholar: [Author Only Title Only Author and Title](#)

McQuaid JB, Kustka AB, Obornik M, Horák A, McCrow JP, Karas BJ, Zheng H, Kindeberg T, Andersson AJ, Barbeau KA, et al (2018) Carbonate-sensitive phytoferritin controls high-affinity iron uptake in diatoms. Nature 555: 534–537

Pubmed: [Author and Title](#)
CrossRef: [Author and Title](#)
Google Scholar: [Author Only Title Only Author and Title](#)

Miloslavina Y, Grouneva I, Lambrev PH, Lepetit B, Goss R, Wilhelm C, Holzwarth AR (2009) Ultrafast fluorescence study on the location and mechanism of non-photochemical quenching in diatoms. Biochim Biophys Acta BBA - Bioenergetics 1787: 1189–1197

Pubmed: [Author and Title](#)
CrossRef: [Author and Title](#)
Google Scholar: [Author Only Title Only Author and Title](#)

Mock T, Otilar RP, Strauss J, McMullan M, Pajanen P, Schmutz J, Salamov A, Sanges R, Toseland A, Ward BJ, et al (2017) Evolutionary genomics of the cold-adapted diatom *Fragilariopsis cylindrus*. Nature 541: 536–540

Pubmed: [Author and Title](#)
CrossRef: [Author and Title](#)
Google Scholar: [Author Only Title Only Author and Title](#)

Morrissey J, Sutak R, Paz-Yepes J, Tanaka A, Moustafa A, Veluchamy A, Thomas Y, Botebol H, Bouget F-Y, McQuaid JB, et al (2015) A Novel Protein, Ubiquitous in Marine Phytoplankton, Concentrates Iron at the Cell Surface and Facilitates Uptake. Curr Biol 25: 364–371

Pubmed: [Author and Title](#)
CrossRef: [Author and Title](#)
Google Scholar: [Author Only Title Only Author and Title](#)

Müller P, Li XP, Niyogi KK (2001) Non-photochemical quenching. A response to excess light energy. Plant Physiol 125: 1558–1566

Pubmed: [Author and Title](#)
CrossRef: [Author and Title](#)
Google Scholar: [Author Only Title Only Author and Title](#)

Nagao R, Takahashi S, Suzuki T, Dohmae N, Nakazato K, Tomo T (2013) Comparison of oligomeric states and polypeptide compositions of fucoxanthin chlorophyll *a/c*-binding protein complexes among various diatom species. Photosynth Res 117: 281–288

Pubmed: [Author and Title](#)
CrossRef: [Author and Title](#)
Google Scholar: [Author Only Title Only Author and Title](#)

Nymark M, Valle KC, Brembu T, Hancke K, Winge P, Andresen K, Johnsen G, Bones AM (2009) An integrated analysis of molecular acclimation to high light in the marine diatom *Phaeodactylum tricornutum*. PloS One 4: e7743

Pubmed: [Author and Title](#)
CrossRef: [Author and Title](#)
Google Scholar: [Author Only Title Only Author and Title](#)

van Oort B, Murali S, Wentjes E, Koehorst RBM, Spruijt RB, van Hoek A, Croce R, van Amerongen H (2009) Ultrafast resonance energy transfer from a site-specifically attached fluorescent chromophore reveals the folding of the N-terminal domain of CP29. Chem Phys 357: 113–119

Pubmed: [Author and Title](#)
CrossRef: [Author and Title](#)
Google Scholar: [Author Only Title Only Author and Title](#)

van Stokkum IHM, Larsen DS, van Grondelle R (2004) Global and target analysis of time-resolved spectra. Biochimica et Biophysica Acta (BBA) - Bioenergetics 1657: 82–104

Pubmed: [Author and Title](#)
CrossRef: [Author and Title](#)
Google Scholar: [Author Only Title Only Author and Title](#)

van Stokkum IHM, Van Oort B, Van Mourik F, Gobets B, Van Amerongen H (2008) (Sub)-Picosecond Spectral Evolution of Fluorescence Studied with a Synchroscan Streak-Camera System and Target Analysis. In TJ Aartsma, J Matysik, eds, Biophys. Tech. Photosynth. Springer Netherlands, Dordrecht, pp 223–240

Pubmed: [Author and Title](#)
CrossRef: [Author and Title](#)

Google Scholar: [Author Only](#) [Title Only](#) [Author and Title](#)

Park Y-I, Chow W, Anderson J (1995) Light inactivation of functional photosystem II in leaves of peas grown in moderate light depends on photon exposure. *Planta*. doi: 10.1007/BF00203636

Pubmed: [Author and Title](#)

CrossRef: [Author and Title](#)

Google Scholar: [Author Only](#) [Title Only](#) [Author and Title](#)

Peers G, Truong TB, Ostendorf E, Busch A, Elrad D, Grossman AR, Hippler M, Niyogi KK (2009) An ancient light-harvesting protein is critical for the regulation of algal photosynthesis. *Nature* 462: 518–521

Pubmed: [Author and Title](#)

CrossRef: [Author and Title](#)

Google Scholar: [Author Only](#) [Title Only](#) [Author and Title](#)

Pinnola A, Cazzaniga S, Alboresi A, Nevo R, Levin-Zaidman S, Reich Z, Bassi R (2015) Light-Harvesting Complex Stress-Related Proteins Catalyze Excess Energy Dissipation in Both Photosystems of *Physcomitrella patens*. *Plant Cell* 27: 3213–3227

Pubmed: [Author and Title](#)

CrossRef: [Author and Title](#)

Google Scholar: [Author Only](#) [Title Only](#) [Author and Title](#)

Ruban A, Lavaud J, Rousseau B, Guglielmi G, Horton P, Etienne A-L (2004) The super-excess energy dissipation in diatom algae: comparative analysis with higher plants. *Photosynth Res* 82: 165–175

Pubmed: [Author and Title](#)

CrossRef: [Author and Title](#)

Google Scholar: [Author Only](#) [Title Only](#) [Author and Title](#)

Schaller-Laudel S, Volke D, Redlich M, Kansy M, Hoffmann R, Wilhelm C, Goss R (2015) The diadinoxanthin diatoxanthin cycle induces structural rearrangements of the isolated FCP antenna complexes of the pennate diatom *Phaeodactylum tricornutum*. *Plant Physiol Biochem* 96: 364–376

Pubmed: [Author and Title](#)

CrossRef: [Author and Title](#)

Google Scholar: [Author Only](#) [Title Only](#) [Author and Title](#)

Schneider CA, Rasband WS, Eliceiri KW (2012) NIH Image to ImageJ: 25 years of image analysis. *Nat Methods* 9: 671–675

Pubmed: [Author and Title](#)

CrossRef: [Author and Title](#)

Google Scholar: [Author Only](#) [Title Only](#) [Author and Title](#)

Smetacek V (1999) Diatoms and the Ocean Carbon Cycle. *Protist* 150: 25–32

Pubmed: [Author and Title](#)

CrossRef: [Author and Title](#)

Google Scholar: [Author Only](#) [Title Only](#) [Author and Title](#)

Szabó M, Lepetit B, Goss R, Wilhelm C, Mustárdy L, Garab G (2008) Structurally flexible macro-organization of the pigment–protein complexes of the diatom *Phaeodactylum tricornutum*. *Photosynth Res* 95: 237–245

Pubmed: [Author and Title](#)

CrossRef: [Author and Title](#)

Google Scholar: [Author Only](#) [Title Only](#) [Author and Title](#)

Taddei L, Stella GR, Rogato A, Bailleul B, Fortunato AE, Annunziata R, Sanges R, Thaler M, Lepetit B, Lavaud J, et al (2016) Multisignal control of expression of the LHCX protein family in the marine diatom *Phaeodactylum tricornutum*. *J Exp Bot* 67: 3939–3951

Pubmed: [Author and Title](#)

CrossRef: [Author and Title](#)

Google Scholar: [Author Only](#) [Title Only](#) [Author and Title](#)

Tian L, Xu P, Chukhutsina VU, Holzwarth AR, Croce R (2017) Zeaxanthin-dependent nonphotochemical quenching does not occur in photosystem I in the higher plant *Arabidopsis thaliana*. *Proc Natl Acad Sci U S A* 114: 4828–4832

Pubmed: [Author and Title](#)

CrossRef: [Author and Title](#)

Google Scholar: [Author Only](#) [Title Only](#) [Author and Title](#)

Ünlü C, Polukhina I, van Amerongen H (2016) Origin of pronounced differences in 77 K fluorescence of the green alga *Chlamydomonas reinhardtii* in state 1 and 2. *Eur Biophys J EBJ* 45: 209–217

Pubmed: [Author and Title](#)

CrossRef: [Author and Title](#)

Google Scholar: [Author Only](#) [Title Only](#) [Author and Title](#)

de Vargas C, Audic S, Henry N, Decelle J, Mahe F, Logares R, Lara E, Berney C, Le Bescot N, Probert I, et al (2015) Eukaryotic plankton diversity in the sunlit ocean. *Science* 348: 1261605–1261605

Pubmed: [Author and Title](#)

CrossRef: [Author and Title](#)

Google Scholar: [Author Only](#) [Title Only](#) [Author and Title](#)

van der Weij-de Wit CD, Dekker JP, van Grondelle R, van Stokkum IHM (2011) Charge separation is virtually irreversible in photosystem II core complexes with oxidized primary quinone acceptor. *J Phys Chem A* 115: 3947–3956

Pubmed: [Author and Title](#)
CrossRef: [Author and Title](#)
Google Scholar: [Author Only](#) [Title Only](#) [Author and Title](#)

Wientjes E, van Stokkum IHM, van Amerongen H, Croce R (2011) The role of the individual Lhcas in photosystem I excitation energy trapping. *Biophys J* 101: 745–754

Pubmed: [Author and Title](#)
CrossRef: [Author and Title](#)
Google Scholar: [Author Only](#) [Title Only](#) [Author and Title](#)

Wlodarczyk LM, Dinc E, Croce R, Dekker JP (2016) Excitation energy transfer in *Chlamydomonas reinhardtii* deficient in the PSI core or the PSII core under conditions mimicking state transitions. *Biochim Biophys Acta* 1857: 625–633

Pubmed: [Author and Title](#)
CrossRef: [Author and Title](#)
Google Scholar: [Author Only](#) [Title Only](#) [Author and Title](#)

Wu H, Cockshutt AM, McCarthy A, Campbell DA (2011) Distinctive Photosystem II Photoinactivation and Protein Dynamics in Marine Diatoms. *PLANT Physiol* 156: 2184–2195

Pubmed: [Author and Title](#)
CrossRef: [Author and Title](#)
Google Scholar: [Author Only](#) [Title Only](#) [Author and Title](#)

Zhu S-H, Green BR (2010) Photoprotection in the diatom *Thalassiosira pseudonana*: Role of LI818-like proteins in response to high light stress. *Biochim Biophys Acta BBA - Bioenerg* 1797: 1449–1457

Pubmed: [Author and Title](#)
CrossRef: [Author and Title](#)
Google Scholar: [Author Only](#) [Title Only](#) [Author and Title](#)